Droplet Sequencing Reveals Virulence Gene Clusters in Oral Biofilm Extracellular Vesicles

Sotaro Takano[1], Naradasu Divya[1], Satoshi Takenawa[1], Yan Kangmin[1], Tomoko Maehara[1], Nobuhiko Nomura[2,3], Nozomu Obana[3,4], Masanori Toyofuku[2,3], Michihiko Usui[5], Wataru Ariyoshi[6], Akihiro Okamoto[1,7,8,9,*]

[1] Research Center for Macromolecules and Biomaterials, National Institute for Materials Science, Tsukuba, Japan, 305-0044
[2] Graduate School of Life and Environmental Sciences, University of Tsukuba, Tsukuba, Japan, 305-8577
[3] Microbiology Research Center for Sustainability, University of Tsukuba, Tsukuba, Japan, 305-8577
[4] Transborder Medical Research Center, Faculty of Medicine, University of Tsukuba, 305-8577
[5] Division of Periodontology, Department of Oral Function, Kyushu Dental University, Kitakyushu, Japan, 803-8580
[6] Division of Infection and Molecular Biology, Department of Health Promotion, Kyushu Dental University, Kokura, Kitakyushu, Japan, 803-8580
[7] Graduate School of Chemical Sciences and Engineering, Hokkaido University, Sapporo, Japan, 060-8628
[8] Graduate School of Science and Engineering, College of Science and Engineering, University of Tsukuba, Tsukuba, Japan, 305-8577
[9] Institute of Innovation for Future Earth (IRFE) and Laboratory for Integrated Science and Materials (LiSM), Tokyo Institute of Technology, Yokohama, Japan, 226-8503

*Akihiro Okamoto
Email: OKAMOTO.Akihiro@nims.go.jp

Competing Interest Statement: The authors, Sotaro Takano and Akihiro Okamoto, applied for patents for the single-particle DNA sequencing method. The authors declare no competing financial interests.

This PDF file includes:

Main Text
Figures 1 to 4
Table 1

Abstract

Bacterial extracellular vesicles (BEVs), produced by a broad spectrum of bacteria, play a crucial role in enhancing intercellular communication through DNA transfer. A vital determinant of their gene transfer efficiency is the gene content diversity within BEVs, an aspect that conventional metagenomics fails to capture. Our study bridges this gap with a novel microdroplet-based sequencing technique that precisely details DNA content within hundreds of individual BEVs. This technique revealed a unique DNA profile in BEVs from the oral pathogen *Porphyromonas gingivalis*, pinpointing specific genomic regions related to DNA integration (e.g., DNA transposition and CRISPR-Cas systems). These enriched genes, overlooked by standard analyses that aggregate total read counts, indicate that our method offers a more focused view into the genetic contents of BEVs. Applying our technique to dental plaque-derived BEVs, we discovered a hundredfold higher prevalence of DNA encapsulation than previously estimated, with over 30% of BEVs containing DNA. Specifically, we identified a substantial presence of O-antigen biosynthesis genes, prominent hotspots of frequent horizontal gene transfer, from *Alcaligenes faecalis*. Given that O-antigens mediate host-bacterial interactions, this gene enrichment in the large fraction of BEVs suggests a potential novel pathway by which BEVs could influence pathogenicity within oral biofilms. Our research unveils critical insights into the potential functions of vesicular DNA in microbial communities, establishing a powerful platform for studying vesicular DNA in microbiomes. This technical breakthrough provides a foundational basis for future research in microbial communication and the development of potential therapeutic or diagnosis strategies.

Significance Statement

BEVs have been studied for decades, yet their roles in nature and disease are just beginning to be appreciated. Our study makes a significant leap in understanding the roles of BEVs as gene transfer vehicles. By developing a microdroplet-based sequencing technique, we have uncovered detailed DNA profiles within individual BEVs, a task beyond the capabilities of conventional metagenomic methods. This breakthrough highlights specific genomic regions enriched in BEVs from pure culture and human dental plaque. Furthermore, the high prevalence of biofilm BEVs enriched in O-antigen biosynthesis genes, suggests a potential impact on the pathogenicity of oral biofilms.

68 This research establishes a new methodological platform for exploring the intricacies of BEV-
69 mediated interactions in a complex microbial community.
70
71 **Main Text**
72 **Introduction**
73 Horizontal gene transfer (HGT), the exchange of genetic materials across different organisms,
74 represents a fundamental mechanism in microbial evolution (1). This process enables bacterial
75 cells to acquire novel phenotypic traits (e.g., antibiotic resistance), fostering rapid adaptations to
76 environmental challenges (2-4). HGT's role extends beyond individual survival, significantly
77 influencing the genetic diversification within microbial populations (5). It allows the sharing and
78 integration of beneficial genes across species barriers (6, 7), catalyzing the emergence of novel
79 capabilities within bacterial communities (2, 8). Bacterial extracellular vesicles (BEVs) have
80 emerged as critical facilitators of HGT (9, 10). These vesicles are produced by both Gram-positive
81 and Gram-negative bacteria, encapsulate and condense diverse biomolecules including DNA (11),
82 and are prevalent in the various habitats (12, 13). The internal molecules in BEVs are generally
83 condensed, secreted and protected from the risks of degradation (14), hence the success rate of
84 gene transfer increases in BEV-mediated transfer (15). BEVs have the potential to transfer genetic
85 material not only within a species but also across phylogenetically distant species (16-18). These
86 characteristics are either superior or complement to other molecular mechanisms (e.g., conjugation
87 and natural transformation), expanding the genetic repertoire and adaptability in microbial
88 communities. However, the specific nature of the genetic material within BEVs has remained
89 largely underexplored, obscured by technical limitations in current genomic analysis methods.
90 A critical factor determining the effectiveness of HGT is the quantity of BEVs containing
91 specific genes (16), underscoring the need to understand which genes are present and the diversity
92 of DNA encapsulated in individual BEVs. However, identifying and characterizing the DNA
93 within BEVs poses significant challenges, as conventional metagenomic methods do not
94 adequately differentiate DNA variations among individual vesicles. BEVs selectively enrich
95 certain DNA pieces (19-21) but vesicles from the same bacterial culture can contain different DNA
96 (22). To address this, we apply a novel single-nanoparticle droplet DNA sequencing (NP-DS)
97 technique, adapted from single-cell genomic methodologies (23-25). Applied to BEVs from
98 *Porphyromonas gingivalis* and human dental plaque, genetic contents in individual vesicles were

99 profiled. Given this organism and its BEVs have been implicated in periodontitis and systemic
100 diseases (26, 27), our study points to specific aspects of BEV-derived DNA that may play
101 important functional roles in microbial interactions, particularly in the context of oral biofilms and
102 infection.
103
104 **Results**
105 **Enrichment of specific genomic regions in BEVs produced by an oral pathogenic bacterium**
106 We first explored the characteristics of DNA sequences in BEVs produced by *P. gingivalis,* a
107 prominent pathogen of periodontitis (28, 29). Nanoparticle tracking analysis (NTA) of the isolated
108 samples detected > 10^9 particles (/mL) stained by lipophilic dye (Fig. S1A), indicating the presence
109 of BEVs in bacterial cell cultures. To understand the composition of the DNA housed within these
110 vesicles, we performed shotgun sequencing for the bulk BEV samples (Fig. 1A), after treating the
111 BEVs with DNase I to remove any external DNA. The sequence reads were widely mapped to the
112 original bacterial genome, but several genomic regions were over-detected (Fig. 1B), suggesting a
113 selective DNA packaging within the BEV population.
114 To test this possibility, we performed whole genome amplification (WGA) for those particles by
115 droplet-based method (23). Each nanoparticle was isolated within a gel bead, facilitating in-gel
116 lysis and WGA (see Materials and Methods). The sample was mixed with agarose so that ≈ 40 %
117 of droplets contained a single nanoparticle (Table 1, Fig. S2, presented as R_t). This process
118 harbored 4.6 % of the droplets contained amplified DNA (stained by SYBR-Green-I, Table 1, Fig.
119 S2, presented as *Ro*). Given that nearly 20 % of the total nanoparticles were lipid-stained (Table
120 1, Fig. S1 and Fig S2, presented as R_b), we could estimate that ≈ 60 % of lipid-stained nanoparticles
121 (BEVs) harbored DNA (Table 1). This substantial population underscores a prevalent DNA
122 packaging process within the BEVs of *P. gingivalis*, highly surpassing the low DNA packaging
123 frequency in BEVs (<1%) previously estimated (22). Using SYBR-Green-I (the dye for nucleic
124 acid) directly to BEVs as a conventional method, we detected only less than 1% of positively
125 stained BEVs by NTA (Fig. S1), which is consistent with previous pure culture study (22).
126 Considering that fluorescence staining sensitivity is contingent on DNA length (30), it was
127 conceivable that most of BEVs might contain DNA segments too short to be detected by this
128 technique, and there would be considerable variations in DNA length among BEV particles.

129 To elucidate the DNA content within individual BEV particles, we performed whole-genome
130 sequencing for the DNA amplified by multiple displacement analysis (MDA). We examined the
131 distribution of sequence reads from 96 droplets and found that wide regions of the host
132 chromosome were detected in at least one of the droplets same as bulk-BEV sequencing (Fig. 1B).
133 However, there were variations in the detected genomic regions among BEV-population in *P.*
134 *gingivalis* (Fig. 1B) and the averagely 51 ± 35 kbp of genomic regions were detected in each
135 droplet (Fig. 1C and Table. S1).
136 While the mapped regions by read sequences from *P. gingivalis*-BEVs were not uniformly
137 distributed among 96 droplets (Fig. 1B), we found a few genomic regions that were significantly
138 over-detected among BEV population (binominal test, $p < 0.01$, see Supporting Materials and
139 Methods) (Fig. 1B). Although there were commonly enriched regions between the bulk-BEV-
140 sequencing and the droplet sequencing of BEVs in *P. gingivalis* (Fig. 1B), some of the frequently
141 mapped regions in bulk-BEV sequencing were not classified as enriched in the criterion of the
142 detected droplets. The deviation between the two approaches was also observed in the prevalence
143 of each protein coding sequences (CDSs) among BEVs. The abundance distribution for 1873
144 CDSs estimated by mapped sequence reads (FPKM) in the bulk-BEV-sequencing is longer-tailed
145 than that estimated by the detected droplets in the NP-DS (Fig. 1D). Consequently, the bulk-BEV-
146 sequencing harbored ≈ 7 times more CDSs regarded as enriched (i.e., outliers in the distribution,
147 see Data S1) than the NP-DS (Fig. 1E). Additionally, 16S rRNA sequence was rarely detected in
148 BEVs of *P. gingivalis* (≈ 2 %, Fig. 1F), suggesting that detecting BEVs by this marker gene is less
149 efficient compared to the other enriched genomic regions in this bacterium. Of note, MDA usually
150 harbors chimeric sequences during the amplification process (31), but we confirmed that such
151 chimeric reads did not harbor qualitative difference in the mapping profiles (Fig. S3 and see
152 Supporting Materials and Methods for details).
153
154 **Enrichment of functional genes in BEVs from oral pathogen**
155 We next probed the functional implications of DNA enrichment within *Porphyromonas*
156 *gingivalis* BEVs. To explore the genes loaded into a large fraction of BEV population, we
157 statistically extracted the over-detected CDSs among 96 droplets in the NP-DS, revealing 39
158 significantly over-represented CDSs out of the 1873 present on the genome (Table S1). Around

159 20 % of the enriched CDSs are related to genome arrangements such as transposase, site-specific
160 integrase, and CRISPR-Cas system (9/39).
161 To further dissect their function, we performed homology search of those enriched CDSs against
162 the UniprotKB/Swiss-Prot database (32), categorized them by Gene Ontology terms (GO terms),
163 and statistically screened the enriched GO terms in BEVs (Fig. 2A and Table S2). Among 497
164 categories, 5 categories were identified as statistically enriched (hypergeometric test, p-value <
165 0.05, see Supporting Materials and Methods). We found that "maintenance of CRISPR repeat
166 elements (GO:0004803)" and "DNA transposition (GO:0006313)" emerged as statistically
167 significant categories, indicating the predominance of genome-arrangement functions in the BEV-
168 derived DNA. The "maintenance of CRISPR repeat elements" category, which is also linked to
169 the "defense response to virus (GO:0051607)", was particularly highlighted by the packaging of
170 an entire CRISPR-Cas gene cluster within an enriched genomic region (Fig. 2B). Also, "cobalamin
171 biosynthetic process (GO: 0009236)", was identified as the enriched functional category (Fig. 2A).
172 All four genes associated with this metabolism are not distributed across the genome but are
173 clustered on the specific locus (Fig. 2C).
174 We also performed the same analysis of genes in bulk-BEV sequencing and confirmed that the
175 same or similar GO terms such as "cobalamin biosynthetic process (GO: 0009236)" and
176 "threonine-phosphate decarboxylase activity (GO:0048472)" were identified (Table. S3). Totally,
177 ≈ 3 times more categories were identified in the bulk-BEV sequencing, including various
178 metabolic, stress-response, and enzymatic categories (Table. S3). The discrepancy between bulk-
179 BEV sequencing and NP-DS results may indicate a significant difference between genes abundant
180 in quantity and those consistently present in a large proportion of BEVs, highlighting the
181 heterogeneity in DNA encapsulation within BEVs.
182
183 **DNA profiling of nanoparticles from human oral biofilm by microdroplet sequencing**
184 We next attempted to characterize DNA content in BEVs produced in the dental plaque biofilm
185 of periodontal patients, the natural habitat of oral pathogenic bacteria. Transmission electron
186 micrographs of the isolated samples revealed that there were spherical particles with diameters ≈
187 of 100 to 200 nm (Fig. S4A). NTA also detected the particles stained by lipophilic fluorescent dye
188 or double-stranded DNA dye (Fig. S4A), but the number of DNA-staining positive particles was
189 greater than those stained by lipid dye (Fig. S4B), implying the presence of nanoparticles with

190 DNA that does not consist of a lipid layer such as viruses. However, the amount of extracted DNA
191 from those treated samples was below the minimum amount required for conventional
192 metagenome sequencing (< 1 ng per sample).
193 Remarkably, our droplet sequencing was successful for the collected BEVs with such low amount
194 of DNA. As with the NP-DS for *P. gingivalis*, the sample was mixed with agarose and lipid
195 staining and SYBR-Green-I were used for the number quantification of BEVs and BEVs with
196 amplified DNA (Fig. S2). We could then estimate the fraction of nanoparticles with DNA is ≈
197 10 % (Fig. S2BC), which is almost identical to the rate of stained particles by DNA-dye in NTA
198 (Fig. S4B). We next sequenced those 384 positive droplets in total (Fig. 3B). Sequence reads from
199 each droplet were computationally assembled and divided into CDS unit and searched against the
200 nr database (see Materials and Methods). This method detected an average of 52 ± 29 CDSs in one
201 droplet (Fig. 3C), most of which were classified as a virus (bacteriophage)-derived CDS (we call
202 this vCDS hereafter). Of 384 droplets we analyzed, ≈ 20 % of droplets (68/384) contained ≥ 5
203 bacterial CDSs (we call these bCDSs hereafter) (Fig. 3D), and those droplets were regarded as
204 BEV-containing droplets, and the rest of the droplets contained mostly vCDSs (295/384). When
205 we take into account the fraction of viral particles estimated by the NP-DS, the ratio of BEVs with
206 DNA is estimated as ≈ 30% (Table 1, Fig. S2B, presented as *r*), and thus a significant fraction of
207 BEVs contained DNA in the oral biofilm. We observe particles with the morphology of tailed
208 bacteriophages in TEM (Fig. S5A), all the vCDSs were assigned to *Caudovirales* (Fig. S5B), and
209 thus the origin of the most of viral DNA would be those phage particles. However, we also
210 observed several droplets containing both bCDSs and vCDSs, and the origin of the viral DNA in
211 such cases will be discussed later.
212 We compared the DNA content in a BEV to that of a bacterial cell by droplet sequencing of
213 bacterial cells (cell-DS) isolated from the same dental plaque samples (Fig. 3B). In cell-DS,
214 averagely 1204 ± 542 CDSs and 790 ± 490 kbp of CDS region was detected (Fig. 3C and Fig.
215 S6A), and full-length 16S rRNA sequences were observed in over 90 % of the droplets (Fig. 3E).
216 In contrast, the CDS regions detected in BEV-containing droplets were mostly around 9 kbp in
217 each droplet (8.6 ± 6.5 kbp, Fig. S6B), corresponding to ≈ 1 % of those detected in cell-DS. Also,
218 full-length 16S rRNA sequences were detected only in 4% (3/68) of BEV-containing droplets (Fig.
219 3E). The length and prevalence of DNA in BEVs from oral plaque biofilms are consistent with
220 those observed in *P. gingivalis*.

221

222 **Enrichment of specific genomic regions in BEVs from the oral cavity**

223 We next taxonomically annotated the detected bCDSs in each droplet by homology search against
224 the GTDB database (Fig. S7). We found that most of the detected bCDSs in each BEV-containing
225 droplet derived from a single phylum, family, and genus-group (around 70 ~ 90% of purity, Fig.
226 4A and Fig. S8), and we assumed that the most frequently detected bacterial taxon (MFT) for each
227 droplet reflects an originating bacterium of a BEV. Mapping of the detected sequence reads to the
228 assembly genome of the MFT (Fig. S7) revealed that most of the BEV-containing droplets
229 contained around 0.5 ~ 1 % of the genomic regions of the MFT, while the droplets in cell-DS
230 reasonably covered an average of 40 ~ 60 % of the genomic regions of MFT (Fig. 4B).

231 The enrichment of specific genomic regions was also observed in BEVs from the dental plaque
232 biofilm as with pure culture system. We focused on droplets whose MFT is *Alcaligenes faecalis*
233 (GCF_002443155.1), which is most frequently observed taxon as MFT in the BEV-containing
234 droplets (Fig. 4C). The mapped regions by sequence reads differed among droplets and distributed
235 to the wide range of the host chromosomal region (Fig. 4C). However, there were commonly
236 detected regions among the droplet (Fig. 4C, binominal test, p-value < 0.01). Among the 46 CDSs
237 located on the enriched regions, many of the genes related to lipopolysaccharide (LPS)
238 biosynthesis (Table S4), and most of those are clustered in one genomic locus (Fig. 4D). A
239 statistical screening of enriched functional categories (GO terms) in those genes revealed that most
240 of the screened GO terms are associated with biosynthesis of bacterial antigen (LPS), such as "O
241 antigen biosynthetic process (GO:0009243)" and "LPS biosynthetic process (GO:0009103)" (Fig.
242 4E and Table S5). "O-antigen biosynthesis genes" were encapsulated in ≈ 14 % of BEVs of
243 *Alcaligenes faecalis* (≈ 10 % of all analyzed DNA-containing BEVs in the oral biofilm), suggesting
244 the prevalence of these gene in the biofilm BEVs.

245

246 **Origins of BEV-derived DNA in dental plaque**

247 Taxonomic profiles of bCDSs detected in NP-DS showed quite different compositions from
248 those detected in cell-DS. In phylum-level, abundantly detected groups in BEV-containing
249 droplets such as *Proteobacteria* were barely detected in cell-DS (Fig. 4A), and thus most of the
250 DNA sequences detected in BEVs derived from bacterial species with very low abundance in
251 dental plaque biofilm. Indeed, *Actinomyces, Peptidiphaga,* and *Streptococcus* were the most

252 frequently detected taxa and MFTs in ≈ 90 % of droplets in cell-DS, while those CDSs were barely
253 detected in NP-DS (only in 6 droplets in total) (Fig. 4A). On the other hand, CDSs from
254 *Alcaligenes* (*Proteobacteria*), the most abundant genus detected in BEV-derived DNA, were quite
255 low in frequency in cell-DS (Fig. 4A). In addition to *Alcaligenes*, we also found the bCDSs from
256 several minor bacterial genus in cell-DS, such as *Prevoteolla, Capnocytophaga, Campylobacter_B,*
257 *Leptotrichia, and Pseudomonas_E*, in NP-DS. Those results suggest that the detected BEV-
258 derived DNA by our method could reveal the distribution of functional genes among particles, but
259 also highlight the taxonomically minor but active producer strains of BEVs in microbiome.
260

261 **Discussion**

262 Understanding the diversity of DNA cargo within BEVs and identifying genes consistently
263 present is crucial for comprehending the role of HGT at the microbiota level. Traditional
264 metagenomic approaches, however, have struggled to accurately characterize such properties. Our
265 study addresses this limitation by employing droplet sequencing analysis, a method that reveals
266 the overlooked complexity of DNA content in BEVs. We found that BEVs typically harbor
267 substantial DNA fragments (ranging from 10 to 50 kb) from the host genome, with certain regions
268 being prevalent across the BEV population, and those enriched genomic regions contain
269 functionally related gene clusters (Fig. 2, and Fig. 4). Our analysis demonstrates a substantial
270 refinement in identifying functionally relevant genes within BEVs using NP-DS, compared to
271 bulk-BEV sequencing (Fig. 1). The latter tends to capture a broader array of miscellaneous gene
272 sets (as detailed in Data S1) and is susceptible to amplification biases during library preparation.
273 It is possible that DNA amplification within individual droplets, combined with count-based
274 statistical analysis, mitigates these biases, leading to a more precise identification of functionally
275 enriched genes within BEVs. Furthermore, the sensitivity of our technique to detect minute
276 quantities of DNA expands the potential of NP-DS for broader application across a variety of
277 microbiome samples.

278 Enrichment profiles and prevalence of DNA content suggest their potential ecological impacts
279 on the microbial community via HGT. The enrichment of a specific group of metabolic or
280 virulence-associated genes was found in both bacterial cases (Fig. 2A and Fig. 4E), which is
281 reminiscent of similarities with other mobile genetic elements (e.g., plasmid and integrative
282 conjugative element) (33, 34). For both cases, clustered gene sets are found to be 3 - 12 % of BEVs,

283 which is a hundred times greater than what was detected in the natural environment using
284 traditional DNA dye staining techniques (22), revealing DNA-packaging BEVs are far more
285 prevalent than previously estimated.

286 "O-anitgen biosynthesis genes" were quite prevalent in the BEVs derived from the oral plaque
287 biofilm. This gene sets are generally clustered on the genome of gram-negative bacteria (35, 36),
288 and high sequence diversity and unique GC content of that genomic region suggests that this gene
289 cluster is a frequent site of HGT (37, 38). Given that divergence in O-antigen have an potential
290 impact on the host-bacterial interactions (39), one possibility is that the enriched genes in BEVs
291 could modulate pathogenicity of the oral biofilm via HGT.

292 In BEVs from *Porphyromonas gingivalis*, we observed the enrichment of genes associated with
293 DNA integration, such as those involved in DNA transposition and CRISPR-Cas systems. The
294 interspecies exchange and transposition of insertion sequences (IS) are believed to contribute to
295 genome rearrangements in this pathogen (40). Intriguingly, the CRISPR spacer sequences are
296 highly homologous to regions of IS on the *P. gingivalis* genome, and those spacer sequences are
297 possibly responsible for preventing IS transposition and recombination (40). The enrichment of
298 both IS and CRISPR-Cas elements suggests that BEVs in this bacterium play an important role in
299 the interspecies recombination of IS and its control by the CRISPR-Cas system by mediating the
300 HGT. While the frequency and extent to which these genes are transferred among bacteria warrant
301 further investigation, our study lays the groundwork by identifying transferable gene candidates
302 via BEVs and their potential effects on microbial community dynamics.

303 Our findings not only highlight the enrichment of the specific genomic locus in BEVs but also
304 revealed considerable variation in the profiles of BEV-containing droplets (Fig. 1B and Fig. 4D),
305 suggesting that the packaging process influenced by both probabilistic and deterministic factors.
306 For *P. gingivalis,* the BEV DNA is notably rich in transposable elements, suggesting that these
307 DNA regions tend to be excised and loaded into the BEVs via certain mechanisms. While the
308 excision of the IS element itself is generally considered as a stochastic event, it can be influenced
309 by environmental stressors or specific genetic factors (41, 42), which may alter the frequency of
310 their incorporation into BEVs (43).

311 Conversely, in other genomic loci where we did not detect signatures of excision, the inclusion of
312 specific DNA fragments into BEVs might not be driven by site-specific excision. In such a case,
313 fragmentation of chromosomal DNA upon explosive cell lysis would be one plausible mechanism

314 for generating small pieces of DNA. The mechanism underlying selective DNA packaging into
315 BEVs may vary; for instance, *Janas et al.* proposed the difference in affinity of an RNA molecule
316 to the membrane as a mechanism for a high abundance of the specific RNA (44). A similar
317 principle could apply to DNA, where molecular affinities and interactions influence the selection
318 process for vesicle encapsulation.

319 While prior research has attempted to identify BEV producers using 16S rRNA sequencing, our
320 findings underscore the rarity of 16S rRNA sequences within BEVs (refer to Fig. 1E and Fig. 3E),
321 highlighting the limitations of 16S rRNA-based taxonomic identification, such as amplicon
322 sequencing. Instead, our droplet-based sequencing method provides a more comprehensive view
323 of the taxonomic composition of BEV-derived DNA, revealing substantial taxonomic difference
324 between the profiles obtained from cell-DS and NP-DS (Fig. 4A). This discrepancy suggests that
325 the minor members more actively produce BEVs or package DNA into BEVs than the major
326 bacterial group in the human dental plaque. NP-DS identified DNA from several other pathogens
327 (e.g., *Capnocytophaga* and *Leptotrichia*), which were quite minor bacterial groups in our cell-DS
328 data (Fig. 4A), but some of those were prominent pathogens in periodontitis (45). Assuming
329 controlled DNA encapsulation into BEV is the reflection of microbial activity, these enriched
330 DNA regions may serve as biomarkers for assessing the activity of such pathogens. Therefore, the
331 unique characteristics of BEV-derived DNA imply their potential applicability for biopsy in
332 diagnosis.

333 Our analysis also detected much of phage-derived DNA in NP-DS. Although the origin of those
334 viral DNA fragments would be mostly phage themselves, around 20 % of droplets contained both
335 bacterial and viral CDSs (i.e., more than 5 bCDSs and vCDSs). Given that the samples were treated
336 with DNase I to remove externally existing DNA, it's plausible that these viral fragments were
337 incorporated into BEVs during phage infection or induction, (21, 46) or by phages targeting BEVs
338 as 'decoy' cells (47). Upon identifying key virulent BEV producers and associated phages, such
339 DNA insertion into BEVs has the potential to be harnessed for regulating HGT in phage therapy
340 applications. While further experimental investigation is necessary to understand the coexistence
341 of bacterial and phage DNA, the droplet sequencing would be a potential tool to explore potential
342 phage-BEV interactions in nature.
343

344 **Materials and Methods**

345 **Isolation and purification of BEVs from *P. gingivalis***

346 *P. gingivalis* W83 was grown in Gifu anaerobic medium at 37°C. To maintain anaerobic
347 conditions, 20 min of N_2/CO_2 (80:20 v/v) gas sparging was performed prior to culture inoculation.
348 The culture was grown at 37 °C until the OD_{600} reached 1.0. Then, the culture was centrifuged for
349 10 min at 7800 rpm and 4 °C. The resulting supernatant was passed through 0.22 μm filters to
350 remove any cell debris. The filtered supernatant was ultracentrifuged for 2 h at 126,000 × g at 4 °C
351 and the resulting pellets were re-suspended in phosphate buffered saline (PBS).

352

353 **DNase I treatment**

354 DNase I (13 units (U) / μL) (NIPPON GENE) was added to a final concentration of 2U to treat
355 the external DNA of nanoparticles. This sample was stored at 37 °C for 30 minutes, followed by
356 DNase I deactivation by heating the sample at 80 °C for 10 minutes.

357

358 **DNA sequencing of bulk BEV samples**

359 We purified DNA from DNase I-treated BEV samples using the Isoplant-II DNA extraction kit
360 (NIPPON GENE) according to the manufacturer's instructions. Sequencing libraries were
361 prepared using the QIAseq FX DNA Library Kit (QIAGEN) according to the manufacturer's
362 protocols and sequenced using the Illumina Nextseq 2000 with 2 × 150 bp configuration. The
363 obtained fastq files were processed using fastp 0.19.5 (48), and the sequence reads were aligned
364 to the assembly genomes of the host bacterium (*P. gingivalis*: GCF_000007585.1) by bowtie2 (49)
365 with option (--sensitive-local).

366

367 **Nanoparticle tracking analysis (NTA)**

368 NTA was performed by ZetaView (Particle Metrix) for the quantification of nanoparticles.
369 Samples were measured by scanning 11 cell positions and capturing 30 frames per second. For
370 measurements using fluorescent signals, 488/500 nm and 660/680 nm laser-filter units were used
371 with the camera setting: Sensitivity: 70 ~ 80; Shutter: 200; Minimum trace length: 15. For
372 measurements in scatter mode, we used the following settings: Sensitivity: 65; Shutter: 200;
373 Minimum trace length: 15. Captured video images were further analyzed using the ZetaView
374 Software.

375

376 **Droplet genome sequencing**

377 Droplet genome sequencing was performed by bitBiome (Japan) as previously described (50),
378 and details were described in Supporting Materials and Methods. Briefly, the cell or nanoparticle
379 suspensions were mixed with 1.5 % agarose solutions so that the expected percentage of positive
380 droplets was ≈ 40 % (23). In the case of cell-DS, the encapsulated cells were further lysed by the
381 lysis solutions in gel beads. The droplets in cell-DS and NP-DS were processed for multiple
382 displacement amplification (MDA) by REPLI-g Single cell Kit (QIAGEN), and the beads were
383 stained with 1× SYBR Green (Thermo Fisher Scientific). Green fluorescence-positive beads were
384 sorted by the FACSMelody cell sorter (BD Bioscience). The collected positive droplets were
385 proceeded to the second round of WGA with the REPLI-g Single Cell Kit. The whole-genome
386 amplified samples with enough DNA were further subjected to the whole-genome sequencing
387 analysis using the Nextera XT DNA Library Prep Kit (Illumina) according to the manufacturer's
388 protocols and sequenced using the Illumina HiSeq.

389

390 **Acquisition of transmission electron micrographs (TEM)**

391 Purified BEV samples were placed onto formvar coated copper grids and negatively stained with
392 2% phosphotungstate acid solution (pH = 7.0) for 60 sec. The grids were analyzed and visualized
393 using JEM-1400 microscope (JEOL Ltd.) operated at an acceleration voltage of 100 kV and
394 imaged by EM-14830RUBY2 CCD camera (JEOL Ltd.).

395

396 **Subjects and dental plaque sample collection for droplet sequencing**

397 We recruited patients with periodontitis, who were classified as generalized stage III-grade C
398 (51). These patients had not taken antimicrobials within 3 months, were non-smokers, and did not
399 have diabetes or any serious systemic disease. The present study was approved by the ethical
400 committee at Kyushu Dental University (ethical approval number: 26-28) and conducted in
401 accordance with the approved guidelines. All participants signed informed consent.

402 The collection of dental plaque biofilm samples (n = 3) was performed based as follows. Rolled
403 cotton was placed next to the teeth to prevent saliva contamination. Supra- and subgingival plaque
404 was collected by a periodontist using a curette without bleeding. The collected dental plaque
405 biofilm sample was immediately resuspended into 1 mL PBS. Then the biofilm was treated with

406 100 µg/mL Proteinase K (QIAGEN) for 1 hour at 37 ºC with vortexing at 20-minutes intervals to
407 degrade extracellular matrices, and the treated sample was centrifuged for 10 minutes at 6000 g at
408 room temperature. The resulting pellet was resuspended into OMNIgene®-ORAL OM-501 (DNA
409 Genotek) and used for cell-DS. The supernatant was passed through 0.22 µm filters to remove any
410 extracellular substrates. The filtered supernatant was ultracentrifuged for 2 h at 200,000 × g at 4 °C,
411 and the resulting pellets were re-suspended in 10 mM HEPES with 0.85 % NaCl.
412
413 **Data analysis in NP-DS and cell-DS**
414 The paired-end read sequences from each droplet were first processed by fastp 0.19.5 and then
415 assembled by SPAdes 3.12.0. The viral contigs were extracted by VIBRANT 1.2.1 (52) to extract
416 viral contigs. Then coding sequences (CDSs), rRNAs, and tRNAs were extracted from the contigs
417 by Prokka 1.14.6 (53). The extracted CDSs were grouped together and clustered by CD-HIT. The
418 clustered CDSs were first annotated by homology search against the National Center for
419 Biotechnology Information (NCBI) non-redundant (nr) database (downloaded on July 1st, 2021)
420 by DIAMOND 2.0.8 (54). For each CDS, the Genbank accession number of the best-hit protein
421 sequence was further used for taxonomic annotation by BASTA (55). The CDSs classified as
422 Bacteria in the kingdom-level were further annotated by homology search against protein
423 sequences in the Genome Taxonomy Database (GTDB) (56) (version r202) by DIAMOND for
424 more strict taxonomic annotation of bacterial CDSs with a threshold in a percent identity ≥ 80 %.
425 Then we eliminated bacterial taxa that were classified as potential contaminants in low-biomass
426 human samples in previous studies (57, 58) (see Data S2). For droplets determined to BEV-
427 containing, we first grouped CDSs by GTDB accession number and calculated the total CDS
428 length assigned to each GTDB taxonomy. Then the most abundantly detected GTDB taxonomy is
429 designated to the "most frequently detected taxon" (MFT) for each droplet. For the details of
430 computational analysis, see the Supporting Materials and Methods.

431
432 **Supporting Information**
433 Supporting Materials and Methods
434 Figs. S1-S8
435 Tables S1-S5

Datasets S1-S2

Acknowledgments

This work was financially supported by JST, PRESTO (JPMJPR19H1 to A.O.), a Grant-in-Aid for Research from the Japan Society for the Promotion of Science KAKENHI (grant numbers 22H02265 to A.O.), and the Japan Agency for Medical Research and Development (19gm6010002h0004 to A.O. and 21ae0121044h0001 to A.O. and So.T.).

Author contributions

So.T. and A.O. designed the research; So.T. developed analysis pipelines and analyzed the data; N.D., Sa.T., Y.K., T.M., M.U., and A. W. performed the experiments; So.T. and A.O. wrote the final version of the paper; All authors contributed to data interpretation and the writing of the manuscript.

Competing interests

The authors, Sotaro Takano and Akihiro Okamoto, applied for patents for the single-particle DNA sequencing method. The authors declare no competing financial interests.

Data availability

All sequence raw data used in this study were deposited in the DNA Data Bank of Japan (DDBJ) with the accession ID PRJDB17260 and PRJDB17266.

Figures and Tables

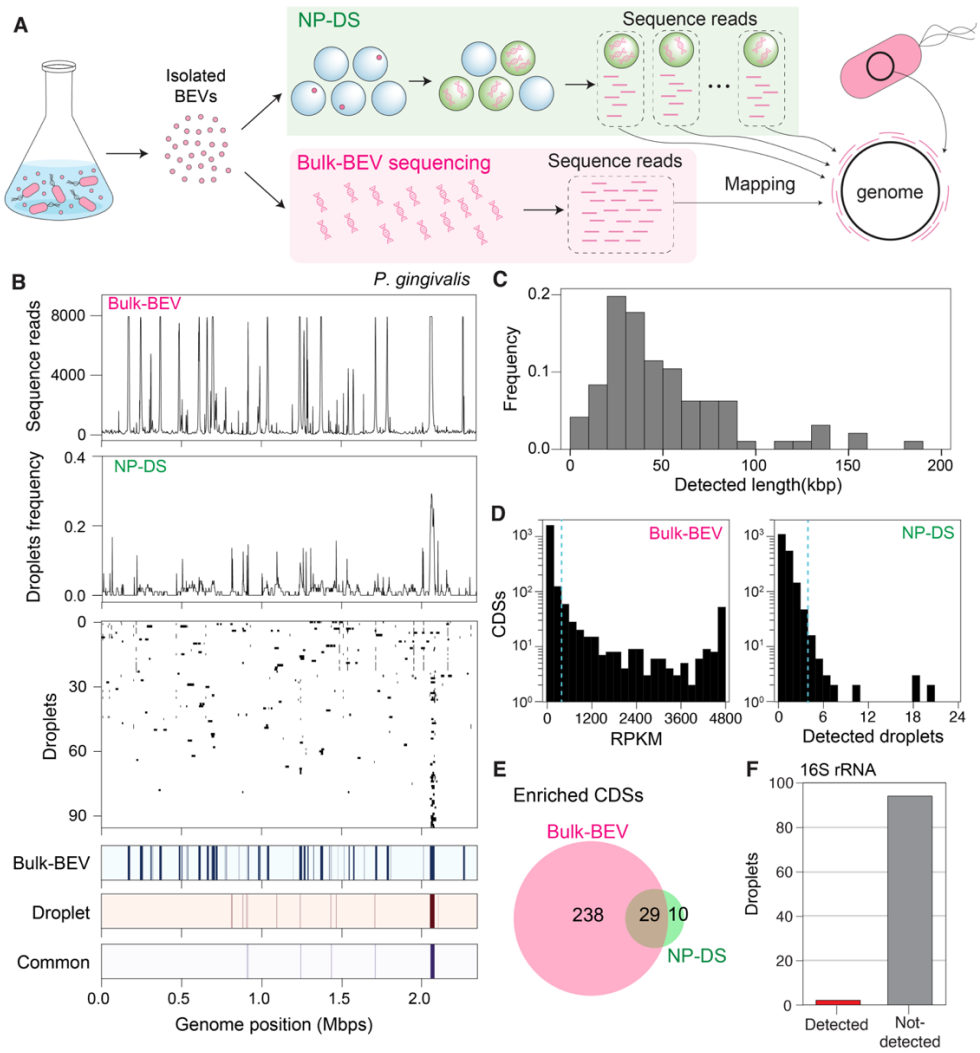

Figure 1 Enrichment of DNA at specific loci of the host genome in *P. gingivalis* BEVs. (A) A schematic of the analysis. For the isolated BEVs from the bacterial culture, we performed nanoparticle droplet sequencing (NP-DS) by DNA amplification of encapsulated droplets or bulk-BEV sequencing by directly extracting DNA from the whole BEV particles for shotgun sequencing. In NP-DS, the collected sequence reads in each droplet was mapped to the original bacterial genome to obtain mapping profiles of individual droplets. In bulk-BEV sequencing, all sequence reads were mapped to the genome collectively. (B) Loci of mapped regions by sequence reads in BEVs on the originating bacterial chromosomes. The number of mapped reads in the next-generation sequencing of the bulk-BEV sample was displayed in a top panel. In the second top panel, the frequency of positive droplets in 96 across each bacterial genome is shown. In the third top panel, the positions on the genome where the sequence reads were mapped in each droplet

471 were filled with black. The genomic regions determined as significantly enriched in bulk-BEVs
472 (more than 75 percentile + 2*IQR (interquartile range)) or droplet sequencing (binominal test, $p <$
473 0.01) were filled with red and blue in the bottom panels, respectively. The enriched chromosomal
474 regions in both the droplet and bulk-BEVs sequence analysis were filled with purple (in the
475 bottom-most panel). (C) The distributions of total length of detected CDSs. (D) The abundance
476 distribution of 1873 CDSs in BEVs. In the bulk-BEV sequencing, the abundance was estimated
477 by the frequency of mapped reads (RPKM). In the case of the NP-DS, the number of droplets
478 detected was used as a metric of the abundance of each CDS. Blue dashed lines indicate the
479 threshold for enriched CDSs (i.e., outliers, 75 percentile + 2*IQR (interquartile range)). (E) Venn
480 diagram for the number of enriched CDSs in the bulk-BEV sequencing and the NP-DS. (F) The
481 percentage of BEV-containing droplets in which 16S rRNA sequence was detected and not
482 detected. The DNA sample is the mixture of BEVs collected from three independent cultures.

483

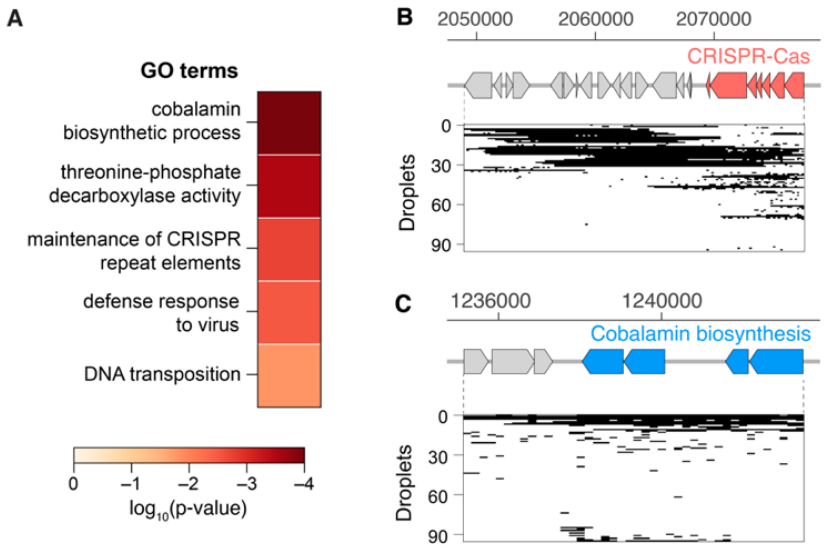

484

485 **Figure 2 Functional enrichment of genes in *P. gingivalis* BEVs.** (A) Enriched gene categories
486 in CDSs detected in BEVs of *P. gingivalis*. Frequently detected CDSs in BEVs were statistically
487 extracted (hypergeometric test, p-value < 0.05, see Supporting Materials and Methods). Gene
488 ontology terms (GO terms) were used for the classification of those frequently detected CDSs.
489 Heatmap indicates the statistical significance level of enrichment. (B), (C) Clustered functional
490 genes located on the enriched genomic regions in *P. gingivalis* BEVs. Detection profiles in 96
491 droplets where (B) CRISPR-Cas gene cluster or (C) cobalamin biosynthetic genes located.

492

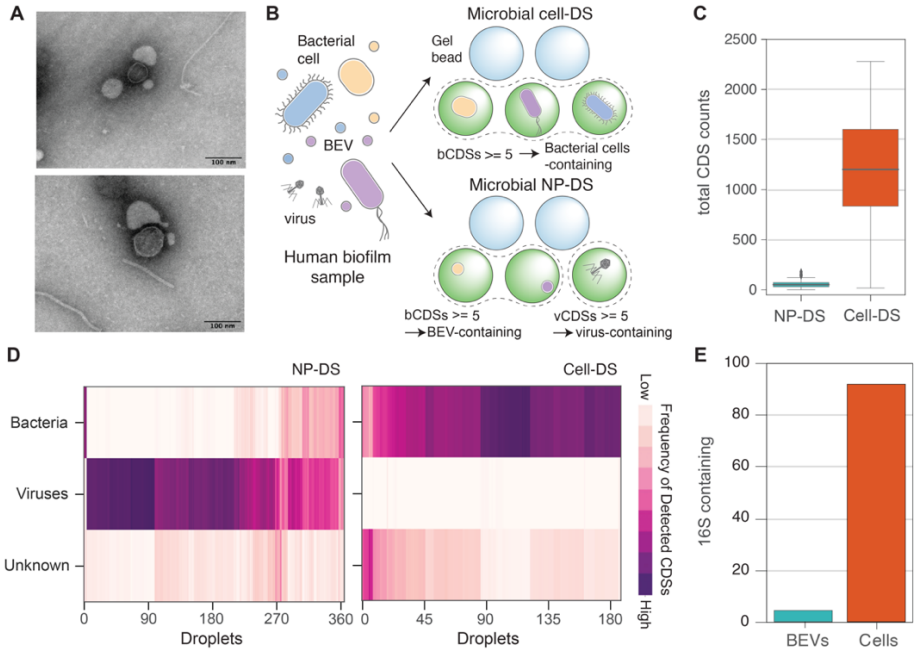

493

494 **Figure 3 Distinct characteristics of DNA in BEVs compared to bacterial cells.** (A) The typical
495 TEM micrographs of BEVs isolated from the dental plaque of periodontal patients. (B) Schematic
496 of microbial cell-DS and NP-DS analysis for the dental plaque biofilm samples from periodontal
497 patients. The separated nanoparticles and bacterial cells in dental biofilms were encapsulated into
498 droplets, and the internal DNA fragments were amplified (see Materials and Methods). In NP-DS,
499 the positive amplification droplets (colored green) were classified by the number of detected
500 bCDSs and vCDSs as BEV-containing, viral DNA-containing, or both. (C) The total length of
501 detected CDSs in NP-DS and cell-DS analysis. The results of all positive droplets from the biofilm
502 samples were analyzed and shown as boxplots. Medians and outliers were shown as bold lines and
503 circles each. (D) Kingdom-level classification of detected CDSs in NP-DS and cell-DS. In each
504 droplet, the length of CDSs assigned to bacteria, viruses, or unknown (i.e., not assigned to any
505 taxon in the database) was normalized by the total length of detected CDSs and shown as a heatmap.
506 The droplets where less than 5 CDSs were detected were eliminated. (E) The percentage of BEV-
507 or bacterial cell-containing droplets in which 16S rRNA sequence was detected. The DNA sample
508 is the mixture of BEVs collected from the biofilm of three patients.

509

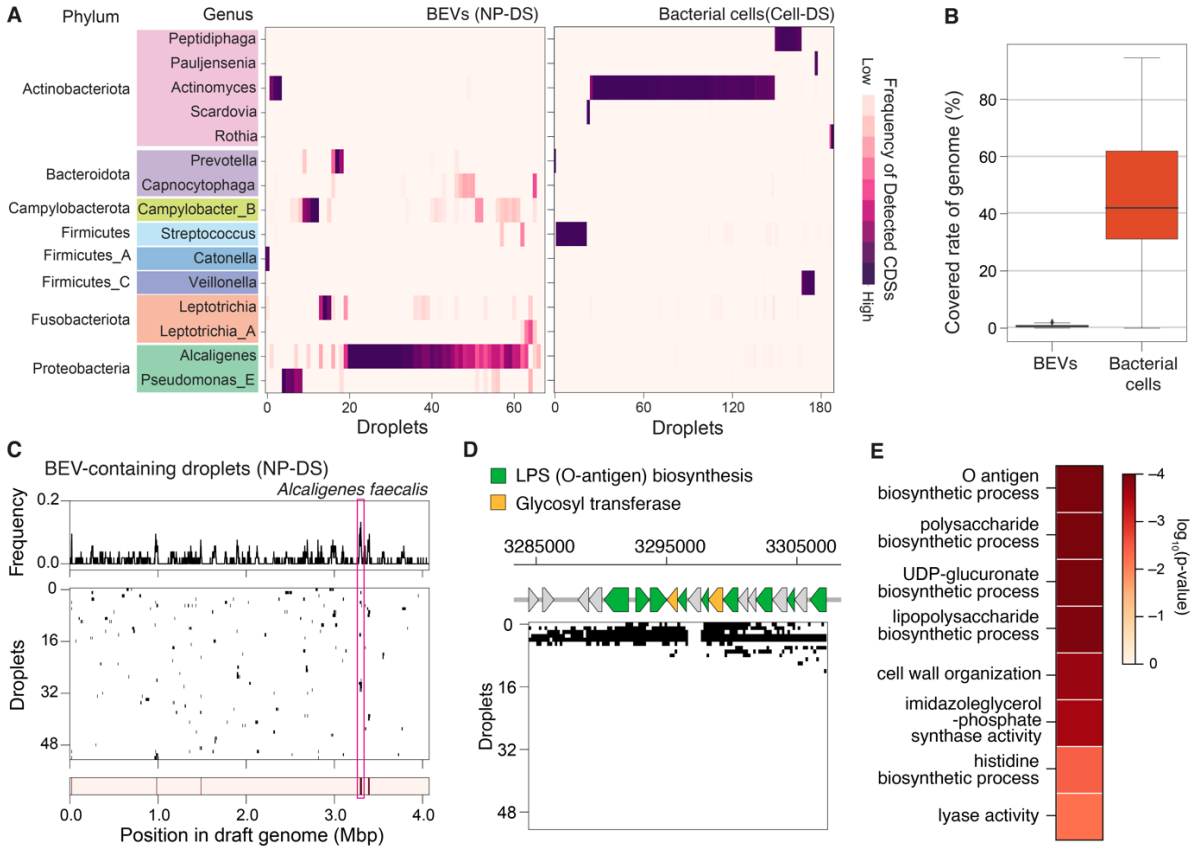

Figure 4 Enriched DNA sequences in BEV-containing droplets. (A) Genus-level taxonomic classification of bCDSs detected in BEV-containing droplets in NP-DS and bacterial cell-containing droplets in cell-DS. The length of CDSs assigned to each bacterial genus group was normalized by the total detected bCDSs and shown as a heatmap. We only showed genera whose maximum frequency of detected CDSs in a single droplet is more than 0.4. (B) The percentage of the genomic region covered by the sequence reads in a BEV- or bacterial cell-containing droplet. For each droplet, sequence reads were aligned to the assembled genome of the MFT. Medians and outliers were shown as bold lines and circles each in box plots. (C) Genomic regions in *Alcaligenes faecalis* (GCF_000745965.1) mapped by sequence reads in BEV-containing droplets. The frequency of droplets including each genomic region (top). The positions on the genome where the sequence reads were mapped in each droplet were filled with black (middle), The genomic regions which were significantly enriched in BEV-containing droplets were filled with red (bottom). We analyzed sequence data of 53 BEV-containing droplets whose MFT was determined as *Alcaligenes faecalis* (GCF_000745965.1). (D) Detection profiles of the LPS biosynthesis gene cluster (encircled by magenta in panel C) in 53 droplets. Green gene arrows correspond to genes

526 associated with LPS (O-antigen) biosynthesis. Yellow gene arrows correspond to glycosyl
527 transferase genes, which are also possibly related to O-antigen biosynthesis process. (E) Screened
528 functional categories (GO terms) as that were significantly overrepresented in the enriched
529 genomic region of BEVs from *Alcaligenes faecalis*. Same as Fig. 1F, we statistically extracted the
530 GO terms (hypergeometric test, p-value < 0.05, see Supporting Materials and Methods). The
531 statistical significance level is shown as a heatmap.
532
533 **Table 1 The percentage of droplets containing amplified DNA fragments after processing**
534 **cells or nanoparticles**. The ratio of droplets to particles with DNA (R_o). The theoretical ratio of
535 droplets to total particles (R_t) was controlled to a fixed value in our analysis. R_o and R_{vb} are
536 estimated by NTA and taxonomic annotation, we calculated the percentage of BEVs with DNA, *r*.
537 For calculation details, see Supporting Materials and Methods and Figure S2.

	R_o	R_t	R_{vb}	R_b	r
P. gingivalis	0.0462	0.361	0	0.206	0.622
Biofilm	0.0352	0.361	4.34	0.0553	0.330

538
539
540
541 **References**
542

543 1. M. F. Polz, E. J. Alm, W. P. Hanage, Horizontal gene transfer and the evolution of
544 bacterial and archaeal population structure. *Trends in Genetics* **29**, 170-175 (2013).
545 2. J. J. Power *et al.*, Adaptive evolution of hybrid bacteria by horizontal gene transfer. *P*
546 *Natl Acad Sci USA* **118** (2021).
547 3. G. L. Peabody, H. Li, K. C. Kao, Sexual recombination and increased mutation rate
548 expedite evolution of in varied fitness landscapes. *Nature Communications* **8** (2017).
549 4. T. F. Cooper, Recombination speeds adaptation by reducing competition between
550 beneficial mutations in populations of *Escherichia coli*. *Plos Biol* **5**, 1899-1905 (2007).
551 5. B. J. Shapiro *et al.*, Population Genomics of Early Events in the Ecological
552 Differentiation of Bacteria. *Science* **336**, 48-51 (2012).
553 6. C. S. Smillie *et al.*, Ecology drives a global network of gene exchange connecting the
554 human microbiome. *Nature* **480**, 241-244 (2011).
555 7. G. Schönknecht *et al.*, Gene Transfer from Bacteria and Archaea Facilitated Evolution of
556 an Extremophilic Eukaryote. *Science* **339**, 1207-1210 (2013).
557 8. T. Y. Pang, M. J. Lercher, Each of 3,323 metabolic innovations in the evolution of arose
558 through the horizontal transfer of a single DNA segment. *P Natl Acad Sci USA* **116**, 187-
559 192 (2019).

560 9. C. Schwechheimer, M. J. Kuehn, Outer-membrane vesicles from Gram-negative bacteria:
561 biogenesis and functions. *Nat Rev Microbiol* **13**, 605-619 (2015).
562 10. I. L. Brito, Examining horizontal gene transfer in microbial communities. *Nat Rev*
563 *Microbiol* **19**, 442-453 (2021).
564 11. M. Toyofuku, N. Nomura, L. Eberl, Types and origins of bacterial membrane vesicles.
565 *Nat Rev Microbiol* **17**, 13-24 (2019).
566 12. J. Tulkens, O. De Wever, A. Hendrix, Analyzing bacterial extracellular vesicles in human
567 body fluids by orthogonal biophysical separation and biochemical characterization. *Nat*
568 *Protoc* **15**, 40-67 (2020).
569 13. S. J. Biller *et al.*, Bacterial vesicles in marine ecosystems. *Science* **343**, 183-186 (2014).
570 14. M. Toyofuku, S. Schild, M. Kaparakis-Liaskos, L. Eberl, Composition and functions of
571 bacterial membrane vesicles. *Nat Rev Microbiol* **21**, 415-430 (2023).
572 15. M. Renelli, V. Matias, R. Y. Lo, T. J. Beveridge, DNA-containing membrane vesicles of
573 Pseudomonas aeruginosa PAO1 and their genetic transformation potential. *Microbiology*
574 *(Reading)* **150**, 2161-2169 (2004).
575 16. F. Tran, J. Q. Boedicker, Genetic cargo and bacterial species set the rate of vesicle-
576 mediated horizontal gene transfer. *Sci Rep* **7**, 8813 (2017).
577 17. S. Fulsundar *et al.*, Gene transfer potential of outer membrane vesicles of Acinetobacter
578 baylyi and effects of stress on vesiculation. *Appl Environ Microbiol* **80**, 3469-3483
579 (2014).
580 18. V. Schaar, T. Nordstrom, M. Morgelin, K. Riesbeck, Moraxella catarrhalis outer
581 membrane vesicles carry beta-lactamase and promote survival of Streptococcus
582 pneumoniae and Haemophilus influenzae by inactivating amoxicillin. *Antimicrob Agents*
583 *Chemother* **55**, 3845-3853 (2011).
584 19. M. V. Surve *et al.*, Membrane Vesicles of Group B Streptococcus Disrupt Feto-Maternal
585 Barrier Leading to Preterm Birth. *PLoS Pathog* **12**, e1005816 (2016).
586 20. N. J. Bitto *et al.*, Bacterial membrane vesicles transport their DNA cargo into host cells.
587 *Sci Rep* **7**, 7072 (2017).
588 21. M. Yasuda *et al.*, Phage Genes Induce Quorum Sensing Signal Release through
589 Membrane Vesicle Formation. *Microbes Environ* **37** (2022).
590 22. S. J. Biller *et al.*, Membrane vesicles in sea water: heterogeneous DNA content and
591 implications for viral abundance estimates. *ISME J* **11**, 394-404 (2017).
592 23. M. Hosokawa, Y. Nishikawa, M. Kogawa, H. Takeyama, Massively parallel whole
593 genome amplification for single-cell sequencing using droplet microfluidics. *Sci Rep* **7**,
594 5199 (2017).
595 24. J. Gole *et al.*, Massively parallel polymerase cloning and genome sequencing of single
596 cells using nanoliter microwells. *Nat Biotechnol* **31**, 1126-1132 (2013).
597 25. E. Z. Macosko *et al.*, Highly Parallel Genome-wide Expression Profiling of Individual
598 Cells Using Nanoliter Droplets. *Cell* **161**, 1202-1214 (2015).
599 26. J. D. Cecil, N. Sirisaengtaksin, N. M. O'Brien-Simpson, A. M. Krachler, Outer
600 Membrane Vesicle-Host Cell Interactions. *Microbiol Spectr* **7** (2019).
601 27. Z. Zhang, D. Liu, S. Liu, S. Zhang, Y. Pan, The Role of Porphyromonas gingivalis Outer
602 Membrane Vesicles in Periodontal Disease and Related Systemic Diseases. *Front Cell*
603 *Infect Microbiol* **10**, 585917 (2020).
604 28. M. H. Ho, C. H. Chen, J. S. Goodwin, B. Y. Wang, H. Xie, Functional Advantages of
605 Porphyromonas gingivalis Vesicles. *PLoS One* **10**, e0123448 (2015).

606 29. R. Nakao *et al.*, Effect of Porphyromonas gingivalis outer membrane vesicles on
607 gingipain-mediated detachment of cultured oral epithelial cells and immune responses.
608 *Microbes Infect* **16**, 6-16 (2014).
609 30. Y. Tomaru, K. Nagasaki, Flow cytometric detection and enumeration of DNA and RNA
610 viruses infecting marine eukaryotic microalgae. *J Oceanogr* **63**, 215-221 (2007).
611 31. R. S. Lasken, T. B. Stockwell, Mechanism of chimera formation during the Multiple
612 Displacement Amplification reaction. *BMC Biotechnol* **7**, 19 (2007).
613 32. E. Boutet, D. Lieberherr, M. Tognolli, M. Schneider, A. Bairoch, UniProtKB/Swiss-Prot.
614 *Methods Mol Biol* **406**, 89-112 (2007).
615 33. M. Gaillard *et al.*, The clc element of Pseudomonas sp. strain B13, a genomic island with
616 various catabolic properties. *J Bacteriol* **188**, 1999-2013 (2006).
617 34. M. G. Durrant, M. M. Li, B. A. Siranosian, S. B. Montgomery, A. S. Bhatt, A
618 Bioinformatic Analysis of Integrative Mobile Genetic Elements Highlights Their Role in
619 Bacterial Adaptation. *Cell Host Microbe* **27**, 140-153 e149 (2020).
620 35. A. Iguchi *et al.*, A complete view of the genetic diversity of the Escherichia coli O-
621 antigen biosynthesis gene cluster. *DNA Res* **22**, 101-107 (2015).
622 36. H. L. Rocchetta, L. L. Burrows, J. S. Lam, Genetics of O-antigen biosynthesis in
623 Pseudomonas aeruginosa. *Microbiol Mol Biol Rev* **63**, 523-553 (1999).
624 37. P. Reeves, Evolution of Salmonella O antigen variation by interspecific gene transfer on
625 a large scale. *Trends Genet* **9**, 17-22 (1993).
626 38. S. E. Hester *et al.*, Horizontally acquired divergent O-antigen contributes to escape from
627 cross-immunity in the classical bordetellae. *BMC Evol Biol* **13**, 209 (2013).
628 39. I. Lerouge, J. Vanderleyden, O-antigen structural variation: mechanisms and possible
629 roles in animal/plant-microbe interactions. *FEMS Microbiol Rev* **26**, 17-47 (2002).
630 40. T. Watanabe *et al.*, CRISPR regulation of intraspecies diversification by limiting IS
631 transposition and intercellular recombination. *Genome Biol Evol* **5**, 1099-1114 (2013).
632 41. P. Siguier, E. Gourbeyre, M. Chandler, Bacterial insertion sequences: their genomic
633 impact and diversity. *Fems Microbiology Reviews* **38**, 865-891 (2014).
634 42. M. Kusumoto *et al.*, Insertion sequence-excision enhancer removes transposable elements
635 from bacterial genomes and induces various genomic deletions. *Nature Communications*
636 **2** (2011).
637 43. N. Orench-Rivera, M. J. Kuehn, Differential Packaging Into Outer Membrane Vesicles
638 Upon Oxidative Stress Reveals a General Mechanism for Cargo Selectivity. *Front*
639 *Microbiol* **12**, 561863 (2021).
640 44. T. Janas, M. M. Janas, K. Sapon, T. Janas, Mechanisms of RNA loading into exosomes.
641 *FEBS Lett* **589**, 1391-1398 (2015).
642 45. E. Kononen, D. Fteita, U. K. Gursoy, M. Gursoy, Prevotella species as oral residents and
643 infectious agents with potential impact on systemic conditions. *J Oral Microbiol* **14**
644 (2022).
645 46. L. Turnbull *et al.*, Explosive cell lysis as a mechanism for the biogenesis of bacterial
646 membrane vesicles and biofilms. *Nat Commun* **7**, 11220 (2016).
647 47. A. J. Manning, M. J. Kuehn, Contribution of bacterial outer membrane vesicles to innate
648 bacterial defense. *BMC Microbiol* **11**, 258 (2011).
649 48. S. Chen, Y. Zhou, Y. Chen, J. Gu, fastp: an ultra-fast all-in-one FASTQ preprocessor.
650 *Bioinformatics* **34**, i884-i890 (2018).

651 49. B. Langmead, S. L. Salzberg, Fast gapped-read alignment with Bowtie 2. *Nature*
652 *Methods* **9**, 357-U354 (2012).
653 50. K. Arikawa *et al.*, Recovery of strain-resolved genomes from human microbiome through
654 an integration framework of single-cell genomics and metagenomics. *Microbiome* **9**, 202
655 (2021).
656 51. J. G. Caton *et al.*, A new classification scheme for periodontal and peri-implant diseases
657 and conditions - Introduction and key changes from the 1999 classification. *J Clin*
658 *Periodontol* **45 Suppl 20**, S1-S8 (2018).
659 52. K. Kieft, Z. Zhou, K. Anantharaman, VIBRANT: automated recovery, annotation and
660 curation of microbial viruses, and evaluation of viral community function from genomic
661 sequences. *Microbiome* **8**, 90 (2020).
662 53. T. Seemann, Prokka: rapid prokaryotic genome annotation. *Bioinformatics* **30**, 2068-2069
663 (2014).
664 54. B. Buchfink, C. Xie, D. H. Huson, Fast and sensitive protein alignment using
665 DIAMOND. *Nat Methods* **12**, 59-60 (2015).
666 55. T. Kahlke, P. J. Ralph, BASTA - Taxonomic classification of sequences and sequence
667 bins using last common ancestor estimations. *Methods Ecol Evol* **10**, 100-103 (2019).
668 56. D. H. Parks *et al.*, A standardized bacterial taxonomy based on genome phylogeny
669 substantially revises the tree of life. *Nat Biotechnol* **36**, 996-1004 (2018).
670 57. G. D. Poore *et al.*, Microbiome analyses of blood and tissues suggest cancer diagnostic
671 approach. *Nature* **579**, 567-574 (2020).
672 58. S. J. Salter *et al.*, Reagent and laboratory contamination can critically impact sequence-
673 based microbiome analyses. *BMC Biol* **12**, 87 (2014).
674
675

676
677
678
679
680
681
682 **Supporting Information for**

683 Droplet Sequencing Reveals Virulence Gene Clusters in Oral Biofilm
684 Extracellular Vesicles

685

686 Sotaro Takano[1], Naradasu Divya[1], Satoshi Takenawa[1], Yan Kangmin[1], Tomoko Maehara[1], Nobuhiko
687 Nomura[2,3], Nozomu Obana[3,4], Masanori Toyofuku[2,3], Michihiko Usui[5], Wataru Ariyoshi[6], Akihiro
688 Okamoto[1,7,8,9]

689

690 [1] Research Center for Macromolecules and Biomaterials, National Institute for Materials Science,
691 Tsukuba, Japan
692 [2] Graduate School of Life and Environmental Sciences, University of Tsukuba, Tsukuba, Japan
693 [3] Microbiology Research Center for Sustainability, University of Tsukuba, Tsukuba, Japan
694 [4] Transborder Medical Research Center, Faculty of Medicine, University of Tsukuba
695 [5] Division of Periodontology, Department of Oral Function, Kyushu Dental University
696 [6] Division of Infection and Molecular Biology, Department of Health Promotion, Kyushu Dental University.
697 [7] Graduate School of Chemical Sciences and Engineering, Hokkaido University, Sapporo, Japan
698 [8] Graduate School of Science and Engineering, College of Science and Engineering, University of
699 Tsukuba
700 [9] Institute of Innovation for Future Earth (IRFE) and Laboratory for Integrated Science and Materials
701 (LiSM), Tokyo Institute of Technology

702

703 Akihiro Okamoto
704 Email: OKAMOTO.Akihiro@nims.go.jp
705

706

707
708
709

710 **Supporting Materials and Methods**

711 **Droplet genome sequencing.**

712 Droplet genome sequencing was performed by bitBiome (Japan) as previously described (1). Briefly, in
713 the cell-DS, the cell suspensions from biofilm samples were mixed with 1.5 % agarose solutions in
714 Dulbecco's PBS (DPBS; Thermo Fisher Scientific) so that the expected percentage of positive droplets was
715 ≈ 40 % (i.e. cells/droplets ratio become ≈ 0.5) based on the previous study (2). In the case of nanoparticle
716 genome sequencing, the suspensions of nanoparticles were mixed with the agarose solutions so that the
717 expected percentage of positive droplets was less than 30 %. Bacterial cells or nanoparticles were
718 encapsulated in droplets using fabricated microfluidic droplet generators (3) and further used for in-bead
719 bacterial genome amplification sequencing. Collected droplets were incubated on ice for 15 min for
720 solidification. The solidified gel droplets were broken with 1H,1H,2H,2H-perfluoro-1-octanol (Sigma-
721 Aldrich). Then, the gel beads were washed with acetone (Sigma-Aldrich), and the solution was mixed
722 vigorously and centrifuged. The gel beads were washed three times each with DPBS, followed by
723 isopropanol. In the case of cell-DS, the encapsulated cells were further lysed by the lysis solutions in gel
724 beads. First, 50 U/ µL Ready-Lyse Lysozyme Solution (Epicentre), 2 U/ mL Zymolyase (Zymo Research),
725 22 U/mL lysostaphin (MERCK), and 250 U/mL mutanolysin (MERCK) were added and incubated in DPBS
726 at 37 °C overnight. Then gel beads were washed three times and 0.5 mg/mL achromopeptidase (FUJIFILM
727 Wako Chemicals) was added into DPBS at 37 °C for 8 hours. The gel beads were washed with DPBS three
728 times again and 1 mg/mL Proteinase K (Promega) with 0.5% SDS in PBS was added and incubated
729 overnight at 40 °C. Following lysis, the gel beads were washed with DPBS five times. Then, the droplets in
730 cell-DS and NP-DS were processed for multiple displacement amplification (MDA) by REPLI-g Single cell
731 Kit (QIAGEN). The droplets were suspended by Buffer D2 from a REPLI-g Single Cell Kit and incubated for
732 2 hours or 8 hours for cell-DS or NP-DS, respectively. Following whole-genome amplification (WGA), gel
733 beads were washed three times with 500 µL DPBS. Thereafter, beads were stained with 1× SYBR Green
734 (Thermo Fisher Scientific) in DPBS. Following the confirmation of DNA amplification by the presence of
735 green fluorescence in the gel, fluorescence-positive beads were sorted into 0.8 µL DPBS in 96-well plates
736 using the FACSMelody cell sorter (BD Bioscience) equipped with a 488-nm excitation laser. Following
737 droplet sorting, 96-well plates were proceeded to the second round of WGA. Second-round MDA was
738 performed with the REPLI-g Single Cell Kit. The 96-well plates were incubated at 65 °C for 10 min after the
739 addition of Buffer D2 (0.6 µL) to each well. Thereafter, 8.6 µL of MDA mixture was added to each well, and
740 the plates were incubated at 30 °C for 2 hours for cell-DS and 8 hours for NP-DS, followed by the incubation
741 at 65 °C for 3 minutes. Following second-round amplification, aliquots of the 96 well-plates were transferred
742 to replica plates for DNA yield quantification using the Qubit dsDNA High Sensitivity Assay Kit (Thermo
743 Fisher Scientific). For cell-DS, 16S rRNA gene Sanger sequencing (FASMAC) with the V3-V4 primers
744 (Forward, 5′-TCGTCGGCAGCGTCAGATGTGTATAA GAGACAGCCTACGGGNGGCWGCAG-3′; reverse,
745 5′-GTCTCGTGGGCTCGGAGATGTGTATAAGAGAC AGGACTACHVGGGTATCTAATCC-3′) was also
746 performed using the replica plates. The whole-genome amplified samples with enough DNA were further

747 subjected to the whole-genome sequencing analysis. In the case of cell-DS, the whole-genome amplified
748 samples were further screened using the Geneious software (Biomatters, Ltd.) based on the quality of 16S
749 rRNA with the criteria that more than 400 bp in length and HQ 40%. For whole-genome sequencing
750 analysis, sequencing libraries were prepared from second-round MDA products using the Nextera XT DNA
751 Library Prep Kit (Illumina) according to the manufacturer's protocols and sequenced using the Illumina
752 HiSeq 2 × 150 bp configuration for the biofilm samples or 2 × 75 bp configuration for *P. gingivalis* BEVs.

753 **Estimation of the percentage of particles with DNA in cell-DS and NP-DS.**

754 The theoretical ratio of droplets to particles in the encapsulation step is denoted as R_t and described as
755 follows:

756 $$R_t = \frac{N}{t}$$

757

758 Here N is the total number of nanoparticles (cells) and t is the number of droplets. We used the fixed R_t for
759 cell-DS or NP-DS as described above. Here, the nanoparticle samples subjected to the gel-lysis are
760 considered as a mixture of viruses, BEVs, and other nanoparticles (extracellular proteins), and thus N can
761 be described as follows:

762 $$N = \alpha + \beta + \gamma + \delta$$

763 Here, α, β, γ, and δ are the total numbers of viruses, BEVs with DNA, BEVs without DNA, and other
764 nanoparticles. The observed ratio of droplets to particles with DNA in the encapsulation step is denoted as
765 R_o and described as follows:

766 $$R_o = \frac{\alpha + \beta}{t}$$

767 For estimating R_o, the percentage of DNA-containing droplets (we call this parameter as P_o hereafter) after
768 processing cells or nanoparticles were quantified by counting the number of droplets with green
769 fluorescence in microscopic images. From P_o, we further estimated the ratio of droplets to particles with
770 DNA (R_o) using the empirical curve in a previous study (2). We can also estimate the ratio of BEVs (R_b) by
771 positive particles by lipid-staining dye using NTA.

772 $$R_b = \frac{\beta + \gamma}{\alpha + \beta + \gamma + \delta}$$

773 The ratio of droplets containing viruses to those containing BEVs with DNA was estimated based on the
774 taxonomic profiles (Fig. 3).

775 $$R_{vb} = \frac{\alpha}{\beta}$$

776 Then the percentage of BEVs with DNA (r) was calculated as follows.

777 $$r = \frac{\beta}{\beta + \gamma} = \frac{R_o}{R_t \cdot R_b(1 + R_{vb})}$$

778

779 **Pre-processing of sequence reads and extraction of CDSs in droplet sequencing**

780 The paired-end read sequences from each droplet were first processed by fastp 0.19.5 (4) for quality
781 control and adapter trimming. The processed sequence reads were assembled by SPAdes 3.12.0 (5) with
782 options (-k auto –disable-rr --careful). The generated contig was used for further processing by VIBRANT
783 1.2.1 (6) to extract viral contigs. Then CDSs, rRNAs, and tRNAs were extracted from the contigs by Prokka
784 1.14.6 (7).
785
786 **Taxonomic annotation of CDSs in droplet sequencing**
787 The extracted CDSs from droplets derived from the same sample were grouped together and clustered
788 by CD-HIT (8) with options (-c 0.98 -s 0.5 -aS 0.9). The clustered CDSs were first annotated by homology
789 search against the National Center for Biotechnology Information (NCBI) non-redundant (nr) database
790 (downloaded on July 1st, 2021) by DIAMOND 2.0.8 (9) with options (--evalue 1e-10 –outfmt 6 –sensitive).
791 For each CDS, the Genbank accession number of the best-hit protein sequence was further used for
792 taxonomic annotation by BASTA (10) with options (sequence prot -l 100 -I 80 -b). At this step, hits whose
793 percent identity is less than 80 % and whose matched length is less than 100 bp were discarded. Genbank
794 accession numbers that were not mapped to the default BASTA database were further mapped to the NCBI
795 database using custom python code implemented in the original BASTA pipeline. Briefly, taxonomic
796 information of each protein sequence in DIAMOND hits was obtained by Bio.Entrez module in Biopython
797 package (11) and formatted by TaxonKit (12).
798 The CDSs classified as Bacteria in the kingdom-level were further annotated by homology search against
799 protein sequences in the Genome Taxonomy Database (GTDB) (13) (version r202) by DIAMOND for more
800 strict taxonomic annotation of bacterial CDSs. If a top-hit of CDS to the GTDB protein database with a
801 percent identity ≥ 80 %, the assembly accession number registered in GTDB was assigned. We eliminated
802 bacterial taxa that were classified as potential contaminants in low-biomass human samples in previous
803 studies (14, 15). The list of eliminated GTDB taxa is shown in Data. S2.
804
805 **Screening of most frequently detected taxon in BEV-containing droplets**
806 For droplets determined to BEV-containing, we first grouped CDSs by their taxonomic information (GTDB
807 accession number) and calculated the total CDS length assigned to each GTDB taxonomy. Then the most
808 abundantly detected GTDB taxonomy in the total CDS length is designated to the "most frequently detected
809 taxon" (MFT) for each droplet.
810
811 **Screening of enriched genomic regions in BEVs from dental plaque biofilm**
812 We first aligned sequence reads obtained from each droplet to the assembly genomes of host bacteria by
813 bowtie2 (16) with option (--sensitive-local). We analyzed BEV-containing droplets from the *P. gingivalis* and
814 mapped the sequence reads to the host bacterial genome (*P. gingivalis*: GCF_000007585.1). It is well
815 known that MDA usually harbors chimeric sequences during the amplification process (17) and it is possible
816 that presence of those chimeric reads affect the mapping profiles. We checked this possibility by BWA (18)

817 and found that only 1.41 ± 0.34 % of reads were classified as chimeric in 96 droplets. We also confirmed
818 that cleaning of those chimeric reads by recently developed algorithm (19) did not harbor qualitative
819 difference in the mapping profiles compared to those generated by the original read sequences (Fig. S3).
820 In the case of BEV-containing droplets in the dental biofilm samples, we focused on *Alcaligenes faecalis*
821 (GCF_002443155.1), which were frequently detected as MFT in droplets. Then, the assembly genome
822 sequences for each bacterium were separated into 1000 bp sections, and significantly enriched genomic
823 regions in the droplets were screened by a binominal test with the following formula:

824 $$p = \sum_{i=k}^{n} \binom{n}{i} {p_0}^k (1 - p_0)^{n-k}$$

825 Where *n* is the total number of droplets examined, *k* is the number of positive droplets (i.e. droplets in which
826 the targeted 1000 bp section was detected), and p_0 is the average frequency of positive droplets for the
827 overall genomic region. If *p* (p-value) is less than 0.01, that 1000 bp section is regarded as an enriched
828 genomic region in BEV-containing droplets.
829
830 **Gene enrichment analysis in BEV-containing droplets**
831 The significantly enriched genomic regions were divided into CDS-unit by Prokka and functionally
832 annotated by homology search using DIAMOND against UniprotKB/Swiss-Prot database (20) (Downloaded
833 on April 21, 2021). To see the enrichment of specific functional categories in BEV-derived CDSs, the gene
834 ontology (GO) annotations (21) are attributed to a top hit in UniprotKB/Swiss-Prot database assigned to
835 each CDS. Then enriched GO annotations in BEV-derived CDSs were screened by a hypergeometric test
836 with the following formula:

837 $$p = \sum_{i=k}^{n} \frac{\binom{G}{i}\binom{G-g}{n-i}}{\binom{G}{n}}$$

838 Where *n* is the total number of enriched CDSs, *G* is the total number of CDSs in the genome, and *g* is the
839 total number of CDSs in a GO annotation category of interest. The probability that more than *k* CDSs were
840 found in each GO annotation category is denoted as *p*. If *p* is less than 0.05, that GO annotation is regarded
841 as an enriched functional category in BEV-containing droplets.
842

843 **Supporting Figures**

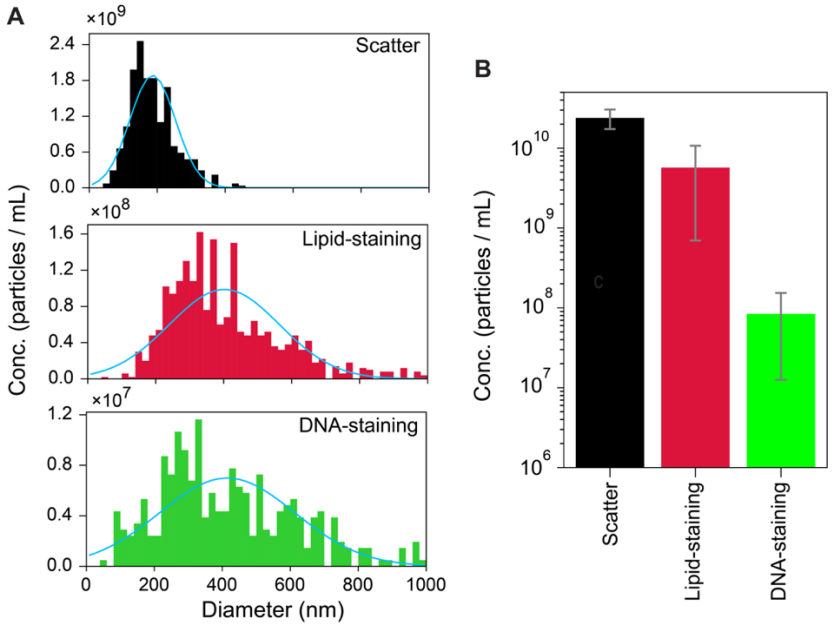

844

845 **Figure S1. NTA (nanoparticle tracking analysis) of BEVs isolated from pure cultures of *P. gingivalis*.**
846 (A) The typical size distribution of nanoparticles isolated from pure cultures of *P.gingivalis* by NTA
847 (nanoparticle tracking analysis). We stained the isolated nanoparticles with the lipid-staining dye, 33.3 μM
848 DiD (1,1'-Dioctadecyl-3,3,3',3'-Tetramethylindodicarbocyanine), and DNA-staining dye, 2.67 μg/mL
849 1000×SYBR-Green I. We detected the scattered light signals (Scatter, black), lipid dye fluorescence (red,
850 detected in 660/680 nm laser-filter unit), or DNA dye fluorescence (green, detected in 488/500 nm laser-
851 filter unit). A blue line is the fitted curve of the normal distribution to the experimental data. (B) The total
852 concentration of nanoparticles detected by each signal with 50 ~ 500 nm in size. Error bars indicate the
853 standard deviations in triplicate experiments.

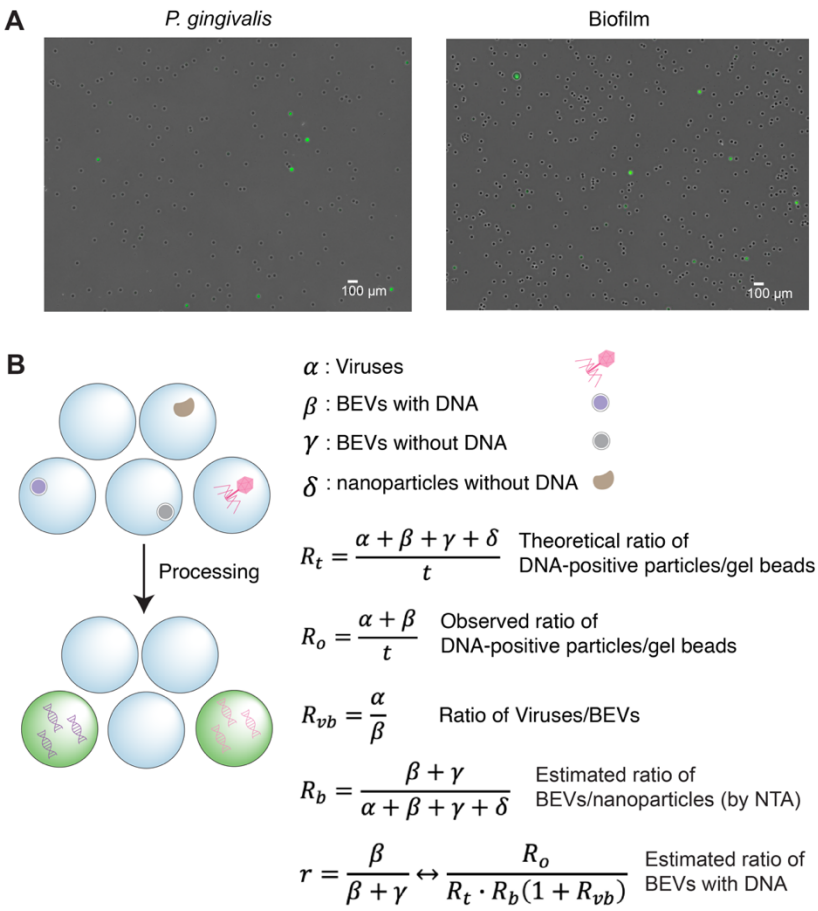

	R_o	R_t	R_{vb}	R_b	r
P. gingivalis	0.0462	0.361	0	0.206	0.622
Biofilm	0.0352	0.361	4.34	0.0553	0.330

Figure S2. The percentage of droplets containing amplified DNA fragments after processing cells or nanoparticles. (A) Representative microscopic fluorescence images of gel beads after in-gel lysis and amplification. The beads were stained by SYBR-Green-I to check the number of positive droplets (i.e., internal DNA was successfully amplified). (B) Schematic of estimating the percentage of nanoparticles with DNA. The nanoparticles expected to contain DNA, BEVs with DNA or phages, were colored by purple and red, respectively. Gel beads expected to contain amplified DNA fragments were colored green. The theoretical ratio of droplets to total particles (R_t) was controlled to a fixed value in our analysis (see Supporting Materials and Methods). The ratio of droplets to particles with DNA (R_o) was estimated by the percentage of positive droplets in a microscopic image and an empirical curve in a previous study. Based on those two parameters and other two parameters estimated by NTA and taxonomic annotation (see Supporting Materials and Methods), we calculated the percentage of BEVs with DNA, *r*. (C) The observed percentage of positive droplets and estimated percentage of BEVs with DNA.

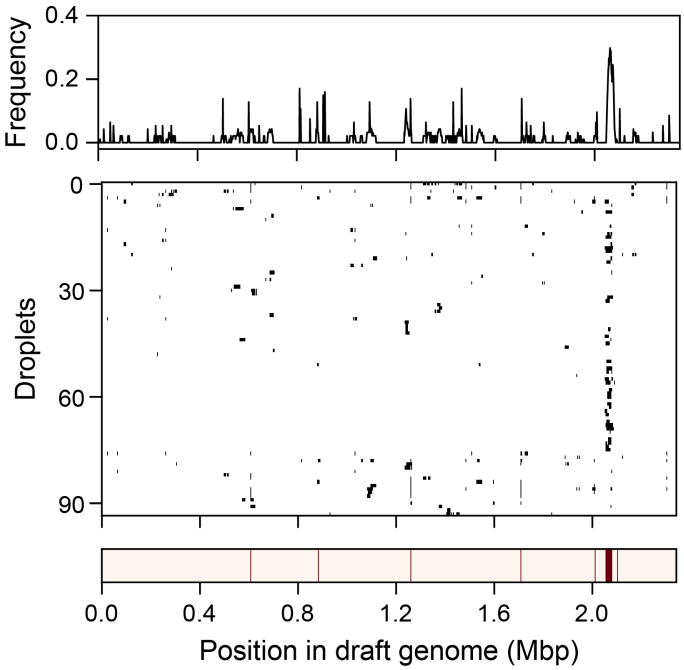

867

868 **Figure S3. Mapping profiles of sequence reads from *P. gingivalis* BEVs after cleaning of chimeric**
869 **reads.** The sequence reads were mapped after the cleaning process of chimeric reads by bwa. Same as
870 Fig. 1B, the genomic positions where the sequence reads were mapped in each droplet were filled with
871 black.

872

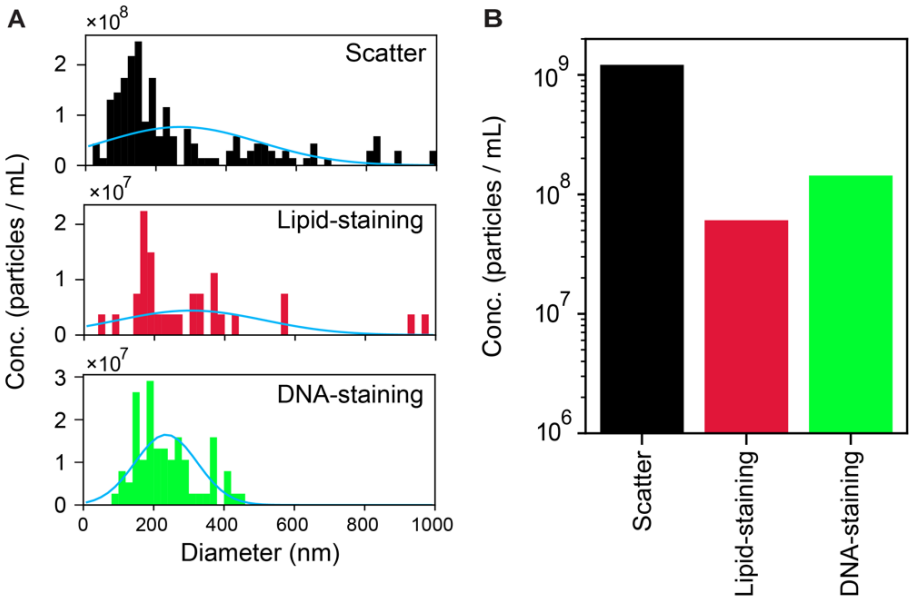

873

874 **Figure S4. Characterization of isolated nanoparticles from the dental plaque biofilm.** (A) The size
875 distribution of nanoparticles isolated from the dental plaque sample. The samples were stained by 5 μg/mL
876 lipid staining FM4-64 for and 1 μg/mL of 1000×SYBR Green I. We detected the scattered light signal (black),

877 lipid dye fluorescence (red, detected in 660/680 nm laser-filter unit), or DNA dye fluorescence (green,
878 detected in 488/500 nm laser-filter unit) by NTA. A blue line is the fitted curve of the normal distribution to
879 the experimental data. (B) The total concentration of particles detected by each signal with 50 ~ 500 nm in
880 size.
881
882

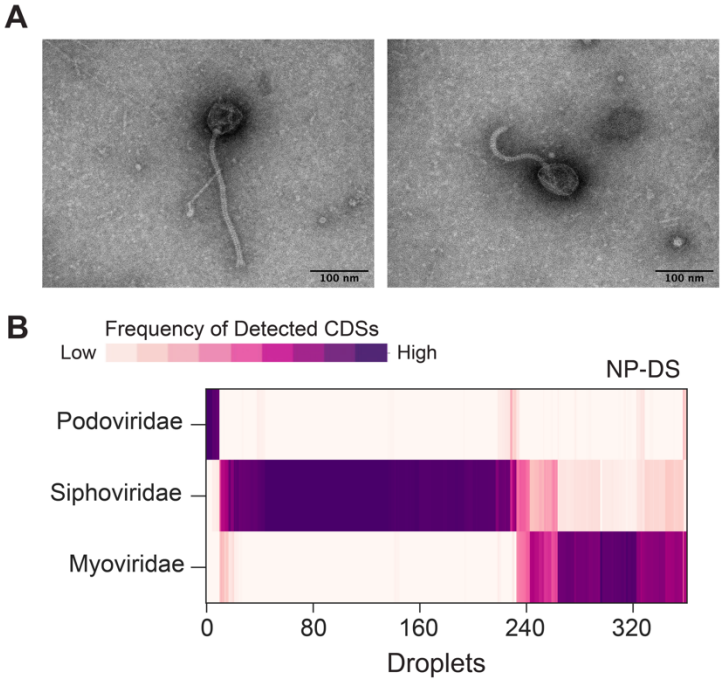

883
884 **Figure S5. Phage particles in an isolated nanoparticle sample from the dental plaque.** (A) The typical
885 TEM micrographs of phage-like particles isolated from the dental plaque of periodontal patients. (B)
886 Taxonomic profiles of phage-derived CDSs detected in NP-DS. Class-level taxonomic classification of viral
887 CDSs (vCDSs) detected in NP-DS was shown as a heatmap. The color of the heatmaps showed the length
888 of CDSs assigned to each taxonomy relative to the total length of vCDS detected in each droplet. We used
889 NCBI taxonomy for classification. Phage species whose maximum frequency of detected CDS length in
890 each droplet is less than 0.4 were not displayed.
891

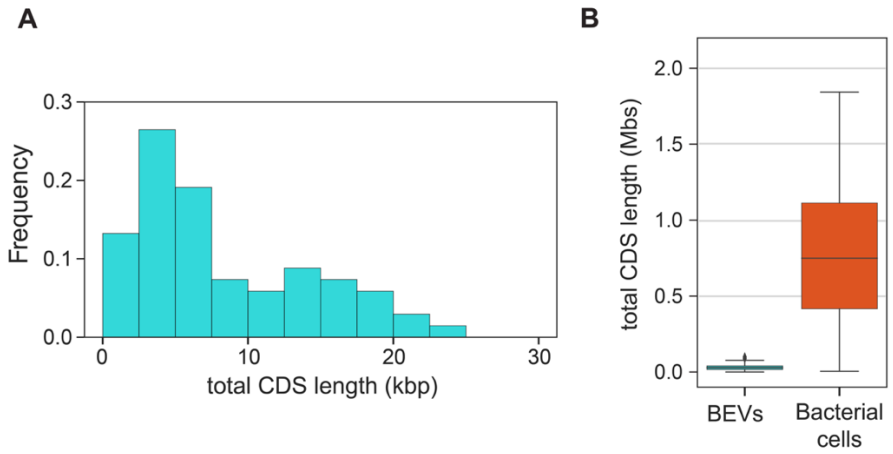

892
893 **Figure S6. Total detected CDS length in BEV-containing droplets.** (A) The distribution of total length
894 of detected bCDS region in BEV-containing droplets. (B) Box plots of total bCDS length in BEV-containing
895 droplets (NP-DS) and bacterial cells containing droplets (cell-DS). Medians and outliers were shown as
896 gray lines and diamonds each.

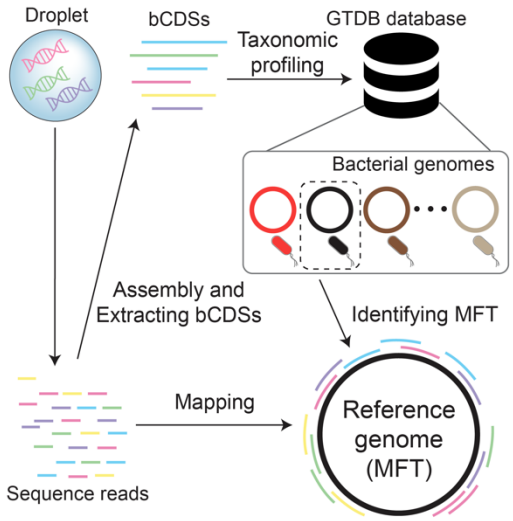

897
898 **Figure S7. A schematic of the analysis for identifying MFT and mapping on the reference genome.**
899 For each droplet, the most frequently detected bacterial taxon (MFT) was identified in GTDB taxonomy
900 based on the annotated information of bCDSs (for details, see Materials and Methods). Then the read
901 sequences were mapped to the corresponding assembly genome of the MFT.

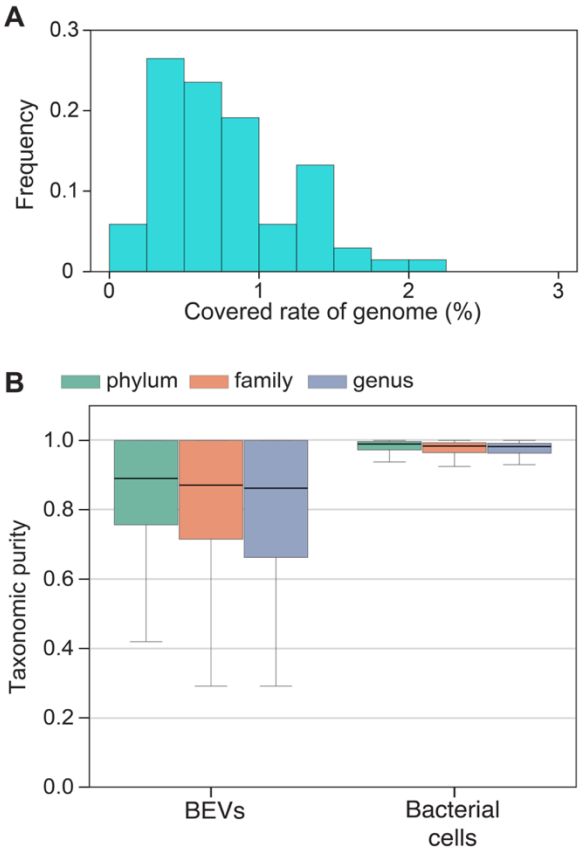

Figure S8. Mapping status of sequence reads in BEV-containing droplets. (A) The distribution of the covered rate of the genome of MFTs by sequence reads in each BEV-containing droplet. (B) Taxonomic purity of detected CDSs in BEVs isolated from the dental plaque. Here, the most frequently detected taxon (MFT) to which BEV-derived CDSs were assigned was first determined, and then the percentage of CDSs length attributed to the MFT in each droplet was calculated and plotted as a boxplot (we call this parameter "purity" of CDSs). We quantified this parameter for the GTDB taxonomic profile in phylum, class, and genus levels. Medians and outliers were shown as gray lines and diamonds each.

913 **Supporting Tables**

Protein id	description	start position (bp)	end position (bp)
WP_013815260.1	hypothetical protein	2062054	2063016
WP_005874812.1	tetratricopeptide repeat protein	2057308	2058195
WP_005874932.1	hypothetical protein	2064777	2066783
WP_230456087.1	2TM domain-containing protein	2058359	2058541
WP_005874833.1	mechanosensitive ion channel	2056208	2057206
WP_230456086.1	T9SS type A sorting domain-containing protein	2058703	2059659
WP_005874913.1	hypothetical protein	2066813	2067403
WP_004583626.1	DNA-binding protein	2051440	2052066
WP_005874827.1	L-threonylcarbamoyladenylate synthase	2052478	2053053
WP_005874926.1	CRISPR-associated endonuclease Cas2	2069305	2069595
WP_005874927.1	hypothetical protein	2073529	2073972
WP_005874822.1	sugar transferase	2053050	2054456
WP_005874906.1	type III-B CRISPR module RAMP protein Cmr6	2072771	2073532
WP_005874912.1	type III-B CRISPR module-associated protein Cmr3	2074684	2075874
WP_010955945.1	IS5 family transposase	216542	217627
WP_005874916.1	CRISPR-associated endonuclease Cas1	2069615	2072710
WP_010956463.1	type III-B CRISPR module RAMP protein Cmr4	2073969	2074670
WP_010955941.1	IS4-like element IS1598 family transposase	199227	200384
WP_005873516.1	threonine-phosphate decarboxylase CobD	1239071	1240078
WP_005873512.1	cob(I)yrinic acid a,c-diamide adenosyltransferase	1241563	1242129
WP_005873514.1	cobyrinate a,c-diamide synthase	1242152	1243471
WP_012458603.1	DUF6261 family protein	2060211	2061263
WP_010956459.1	DUF6261 family protein	2063358	2064410
WP_010956028.1	IS5-like element ISPg8 family transposase	502077	503162
WP_005874030.1	MULTISPECIES: histidinol phosphate phosphatase	611806	612324
WP_005874035.1	purine nucleoside phosphorylase I, inosine and guanosine-specific	615600	616421
WP_005873715.1	histidinol-phosphate aminotransferase	623025	623531
WP_005874530.1	thiamine-phosphate kinase	689154	690194
WP_005873566.1	adenosylcobinamide amidohydrolase	696973	698136
WP_004342769.1	site-specific integrase	878721	879923
WP_004342772.1	hypothetical protein	879930	880292
WP_014709482.1	helix-turn-helix transcriptional regulator	881003	881272
WP_004584269.1	ABC transporter permease	1095538	1096284
WP_005873460.1	ATP-binding cassette domain-containing protein	1096303	1097037
WP_005873451.1	T9SS C-terminal target domain-containing protein	1097132	1098505
WP_004584372.1	S4 domain-containing protein	1236875	1237327
WP_010956235.1	adenosylcobinamide-phosphate synthase CbiB	1238047	1239057
WP_005874841.1	PH domain-containing protein	1374934	1375389
WP_004342775.1	nuclear transport factor 2 family protein	1534837	1535244

914

915 **Table S1. Enriched CDSs in NP-DS of *P. gingivalis* BEVs.** Enriched CDSs of *P. gingivalis* BEVs, which
916 were screened by binominal test (p-value < 0.01). Those screened genes were identical to those screened
917 by the threshold of 75 percentile + 2*IQR (interquartile range).

GO id	category	name	Members in original genome	Members in BEVs	p-value
GO:0009236	P	cobalamin biosynthetic process	13	4	5.02E-05
GO:0048472	F	threonine-phosphate decarboxylase activity	2	2	0.000314
GO:0043571	P	maintenance of CRISPR repeat elements	4	2	0.00185
GO:0051607	P	defense response to virus	5	2	0.00304
GO:0006313	P	DNA transposition	11	2	0.0157

Table S2. Enriched gene categories in NP-DS of *P. gingivalis* BEVs. Enriched GO terms in the enriched CDSs in the BEVs were statistically screened (hypergeometric distribution test, p-value < 0.05). GO terms were grouped into three categories: M: Molecular functions; B: Biological processes; and C: Cellular components.

GO id	category	name	Members in original genome	Members in BEVs	p-value
GO:0009236	P	cobalamin biosynthetic process	15	10	1.28E-06
GO:0015420	F	ABC-type vitamin B12 transporter activity	4	4	0.000243
GO:0043171	P	peptide catabolic process	6	4	0.00297
GO:0032259	P	methylation	10	5	0.00442
GO:0042026	P	protein refolding	4	3	0.00715
GO:0042351	P	'de novo' GDP-L-fucose biosynthetic process	2	2	0.0158
GO:0048472	F	threonine-phosphate decarboxylase activity	2	2	0.0158
GO:0000156	F	phosphorelay response regulator activity	2	2	0.0158
GO:0070009	F	serine-type aminopeptidase activity	2	2	0.0158
GO:0008641	F	ubiquitin-like modifier activating enzyme activity	2	2	0.0158
GO:0022857	F	transmembrane transporter activity	13	5	0.0164
GO:0006541	P	glutamine metabolic process	10	4	0.0276
GO:0009399	P	nitrogen fixation	3	2	0.0435
GO:0009408	P	response to heat	3	2	0.0435

Table S3. Enriched gene categories in bulk-BEV sequencing of *P. gingivalis*. Enriched GO terms screened in the bulk-BEV sequencing data (hypergeometric distribution test, p-value < 0.05).

Protein id	description	start position (bp)	end position (bp)
WP_042487686.1	glycolate oxidase subunit GlcF	981833	983053
WP_042487683.1	hypothetical protein	983361	984668
WP_009454582.1	zeta toxin family protein	1484000	1484545
WP_009454580.1	hypothetical protein	1484541	1484726
WP_042480022.1	helix-turn-helix transcriptional regulator	1484954	1485787
WP_042480881.1	efflux RND transporter periplasmic adaptor subunit	1896312	1897547
WP_042480884.1	ABC transporter ATP-binding protein	1897858	1898649
WP_042487215.1	3-(3-hydroxy-phenyl)propionate transporter MhpT	2690924	2692165
WP_042487212.1	hypothetical protein	2692500	2693114
WP_042486227.1	chlorohydrolase family protein	2981930	2983414
WP_042486230.1	tripartite tricarboxylate transporter substrate-binding protein	2983444	2984421
WP_042486802.1	aspartate/glutamate racemase family protein	3284430	3285188
WP_042486928.1	LysR substrate-binding domain-containing protein	3285492	3286376
WP_226791390.1	ABC transporter permease	3288210	3289034
WP_042486807.1	ABC transporter substrate-binding protein	3289037	3290047
WP_157766853.1	acyltransferase family protein	3290206	3292086
WP_054513292.1	Wzz/FepE/Etk N-terminal domain-containing protein	3292644	3293687
WP_042486816.1	exopolysaccharide biosynthesis polyprenyl glycosylphosphotransferase	3293751	3295019
WP_042486818.1	glycosyltransferase	3295032	3295835
WP_123794683.1	hypothetical protein	3295838	3296524
WP_054513305.1	IS5 family transposase	3296656	3297621
WP_054513289.1	hypothetical protein	3297683	3298210
WP_042486050.1	glycosyltransferase	3298210	3299310
WP_080723785.1	N-acetyl sugar amidotransferase	3299357	3300478
WP_042486045.1	AglZ/HisF2 family acetamidino modification protein	3300478	3301236
WP_042486042.1	imidazole glycerol phosphate synthase subunit HisH	3301236	3301850
WP_052362964.1	lipopolysaccharide biosynthesis protein	3301850	3303094
WP_042486039.1	DegT/DnrJ/EryC1/StrS family aminotransferase	3303137	3304228
WP_042486036.1	UDP-2-acetamido-3-amino-2,3-dideoxy-D-glucuronate N-acetyltransferase	3304228	3304815
WP_042486033.1	Gfo/Idh/MocA family oxidoreductase	3304815	3305759
WP_080723784.1	O-antigen ligase family protein	3305990	3307249
WP_042485889.1	LysR substrate-binding domain-containing protein	3379553	3380554
WP_042485886.1	tRNA 2-selenouridine(34) synthase MnmH	3380547	3381638
WP_042485881.1	NosR/NirI family protein	3381813	3384071
WP_042485877.1	TAT-dependent nitrous-oxide reductase	3384137	3386038

WP_226791393.1	nitrous oxide reductase family maturation protein NosD	3386049	3387386
WP_042485874.1	ABC transporter ATP-binding protein	3387373	3388281
WP_042485871.1	ABC transporter permease	3388288	3389115
WP_042485868.1	nitrous oxide reductase accessory protein NosL	3389115	3389627
WP_042485865.1	FAD:protein FMN transferase	3389663	3390667
WP_042485861.1	glucose-6-phosphate isomerase	3390760	3392328
WP_042485854.1	LTA synthase family protein	3393190	3394734
WP_042485851.1	SDR family NAD(P)-dependent oxidoreductase	3394727	3395497
WP_042485848.1	glycosyltransferase	3395487	3396956
WP_042485845.1	glycosyltransferase	3396975	3398057
WP_042485842.1	glycosyltransferase family 4 protein	3398057	3399370

Table S4. Enriched CDSs of *Alcaligenes faecalis* BEVs. CDSs detected in the enriched genomic region of *Alcaligenes faecalis* BEVs (p-value < 0.01, binominal test). CDS regions were extracted by Prokka and searched against the reference protein fasta file.

GO id	category	name	Members in original genome	Members in BEVs	p-value
GO:0009243	P	O antigen biosynthetic process	9	5	9.30E-10
GO:0000271	P	polysaccharide biosynthetic process	4	4	1.44E-09
GO:0006065	P	UDP-glucuronate biosynthetic process	3	3	2.59E-07
GO:0009103	P	lipopolysaccharide biosynthetic process	15	3	0.000112
GO:0071555	P	cell wall organization	46	4	0.000198
GO:0000107	F	imidazoleglycerol-phosphate synthase activity	4	2	0.000258
GO:0000105	P	histidine biosynthetic process	14	2	0.00375
GO:0016829	F	lyase activity	18	2	0.0062

Table S5. Enriched gene categories of *Alcaligenes faecalis* BEVs. Enriched GO terms in the enriched CDSs in the BEVs of *Alcaligenes faecalis* were statistically screened (hypergeometric distribution test, p-value < 0.05).

Dataset S1 (separate file .xlsx format). Enriched CDSs in bulk BEV-sequencing of *P. gingivalis* BEVs. We screened genes whose FPKM were larger than the threshold (75 percentile + 2*IQR (interquartile range).

Dataset S2 (separate file .xlsx format). A list of all possible sources of contaminant DNA. All the species information in GTDB and NCBI formats were based on the listed taxa in either of Salter *et al.,* 2014 or Poore *et al.,* 2020 (14, 15). The DNA fragments that were taxonomically assigned to one of the listed accession numbers were eliminated.

SI References

1. K. Arikawa *et al.*, Recovery of strain-resolved genomes from human microbiome through an integration framework of single-cell genomics and metagenomics. *Microbiome* **9**, 202 (2021).
2. M. Hosokawa, Y. Nishikawa, M. Kogawa, H. Takeyama, Massively parallel whole genome amplification for single-cell sequencing using droplet microfluidics. *Sci Rep* **7**, 5199 (2017).
3. M. Hosokawa *et al.*, Strain-level profiling of viable microbial community by selective single-cell genome sequencing. *Sci Rep* **12**, 4443 (2022).
4. S. Chen, Y. Zhou, Y. Chen, J. Gu, fastp: an ultra-fast all-in-one FASTQ preprocessor. *Bioinformatics* **34**, i884-i890 (2018).
5. A. Bankevich *et al.*, SPAdes: a new genome assembly algorithm and its applications to single-cell sequencing. *J Comput Biol* **19**, 455-477 (2012).
6. K. Kieft, Z. Zhou, K. Anantharaman, VIBRANT: automated recovery, annotation and curation of microbial viruses, and evaluation of viral community function from genomic sequences. *Microbiome* **8**, 90 (2020).
7. T. Seemann, Prokka: rapid prokaryotic genome annotation. *Bioinformatics* **30**, 2068-2069 (2014).
8. L. Fu, B. Niu, Z. Zhu, S. Wu, W. Li, CD-HIT: accelerated for clustering the next-generation sequencing data. *Bioinformatics* **28**, 3150-3152 (2012).
9. B. Buchfink, C. Xie, D. H. Huson, Fast and sensitive protein alignment using DIAMOND. *Nat Methods* **12**, 59-60 (2015).
10. T. Kahlke, P. J. Ralph, BASTA - Taxonomic classification of sequences and sequence bins using last common ancestor estimations. *Methods Ecol Evol* **10**, 100-103 (2019).
11. P. J. Cock *et al.*, Biopython: freely available Python tools for computational molecular biology and bioinformatics. *Bioinformatics* **25**, 1422-1423 (2009).
12. W. Shen, H. Ren, TaxonKit: A practical and efficient NCBI taxonomy toolkit. *J Genet Genomics* **48**, 844-850 (2021).
13. D. H. Parks *et al.*, A standardized bacterial taxonomy based on genome phylogeny substantially revises the tree of life. *Nat Biotechnol* **36**, 996-1004 (2018).
14. G. D. Poore *et al.*, Microbiome analyses of blood and tissues suggest cancer diagnostic approach. *Nature* **579**, 567-574 (2020).
15. S. J. Salter *et al.*, Reagent and laboratory contamination can critically impact sequence-based microbiome analyses. *BMC Biol* **12**, 87 (2014).
16. B. Langmead, S. L. Salzberg, Fast gapped-read alignment with Bowtie 2. *Nature Methods* **9**, 357-U354 (2012).
17. R. S. Lasken, T. B. Stockwell, Mechanism of chimera formation during the Multiple Displacement Amplification reaction. *BMC Biotechnol* **7**, 19 (2007).
18. H. Li, R. Durbin, Fast and accurate long-read alignment with Burrows-Wheeler transform. *Bioinformatics* **26**, 589-595 (2010).
19. M. Kogawa, M. Hosokawa, Y. Nishikawa, K. Mori, H. Takeyama, Obtaining high-quality draft genomes from uncultured microbes by cleaning and co-assembly of single-cell amplified genomes. *Sci Rep-Uk* **8** (2018).
20. E. Boutet, D. Lieberherr, M. Tognolli, M. Schneider, A. Bairoch, UniProtKB/Swiss-Prot. *Methods Mol Biol* **406**, 89-112 (2007).
21. M. Ashburner *et al.*, Gene ontology: tool for the unification of biology. The Gene Ontology Consortium. *Nat Genet* **25**, 25-29 (2000).